Biogeosciences
Discussions

Open Access

New insights into the organic carbon export in the Mediterranean Sea from 3-D modeling

A. Guyennon[1], M. Baklouti[1], F. Diaz[1], J. Palmieri[2], J. Beuvier[3,4],
C. Lebaupin-Brossier[4], T. Arsouze[5,6], K. Béranger[5], J.-C. Dutay[7], and T. Moutin[1]

[1]Aix Marseille Université, CNRS/INSU, Université de Toulon, IRD, Mediterranean Institute of Oceanography (MIO) UM110, 13288, Marseille, France
[2]Southampton University – National Oceanography Center (NOC), Waterfront Campus, European Way, Southampton SO14 3ZH, UK
[3]Mercator Ocean, Ramonville Saint-Agne, France
[4]CNRM-GAME, Météo-France/CNRS, Toulouse, France
[5]UME, ENSTA-ParisTech, Palaiseau, France
[6]Laboratoire de Météorologie Dynamique, École Polytechnique, Palaiseau, France
[7]LSCE/IPSL, Laboratoire des Sciences du Climat et de l'Environnement, CEA-CNRS-UVSQ, Gif-sur-Yvette, France

Title Page

Abstract	Introduction
Conclusions	References
Tables	Figures

|◀ | ▶|
◀ | ▶

Back | Close

Full Screen / Esc

Printer-friendly Version

Interactive Discussion

New insights into the organic carbon export in the Mediterranean Sea from 3-D modeling

A. Guyennon et al.

Full Screen / Esc

Printer-friendly Version

Interactive Discussion

Abstract

The Mediterranean Sea is one of the most oligotrophic regions of the oceans, and nutrients have been shown to limit both phytoplankton and bacterial activities. This has direct implications on the stock of dissolved organic carbon (DOC), whose high variability
⁵ has already been well-documented even if measurements are still sparse and are associated with important uncertainties. We here propose a Mediterranean Basin-scale view of the export of organic carbon, under its dissolved and particulate forms. For this purpose, we have used a coupled model combining a mechanistic biogeochemical model (Eco3M-MED) and a high-resolution (eddy-resolving) hydrodynamic simulation
¹⁰ (NEMO-MED12). This is the first Basin-scale application of the biogeochemical model Eco3M-MED and is shown to reproduce the main spatial and seasonal biogeochemical characteristics of the Mediterranean Sea. Model estimations of carbon export are of the same order of magnitude as estimations from in situ observations, and their respective spatial patterns are consistent with each other. As for surface chlorophyll, nutrient
¹⁵ concentrations, and productivity, strong differences between the Western and Eastern Basins are evidenced by the model for organic carbon export, with only 39 % of organic carbon (particulate and dissolved) export taking place in the Western Basin. The major result is that except for the Alboran Sea, dissolved organic carbon (DOC) contribution to organic carbon export is higher than that of particulate (POC) in the whole Basin,
²⁰ especially in the Eastern Basin. This paper also investigates the seasonality of DOC and POC exports as well as the differences in the processes involved in DOC and POC exports.

1 Introduction

The biological pump is recognized as a major component of carbon export by the ocean
²⁵ and plays a significant role in the carbon cycle as a whole (Siegenthaler and Sarmiento, 1993). The sinking of organic particles has long been identified as the main process

involved in the biological pump, sustaining the vertical carbon and nutrient gradients in the ocean (Sarmiento and Gruber, 2006; Eppley and Peterson, 1979). Major attention has therefore been paid to the export of organic carbon under its particulate form, as this is the end of the carbon pathway.

The improvement of the characterization of dissolved organic pools (as highlighted by Hansell et al., 2009) led to investigation into the dissolved organic carbon (DOC) compartment in the ocean carbon cycle. As a non-sinking tracer, DOC fate is strongly linked to physical processes and its export occurs via vertical mixing and/or down-welling when it reaches intermediate waters, and via oceanic overturning circulation when it reaches the deepest layers (Hansell et al., 2002). If the early works of Copin-Montégut and Avril (1993) in the Mediterranean Sea and Carlson et al. (1994) in the Sargasso Sea were the first attempts to evaluate the export of DOC below the euphotic zone, the estimation of particulate organic carbon (POC) export calculation had begun years before with the deployment of sediment traps and isotopics following (Buesseler, 1991).

The seasonal variability of DOC in the euphotic zone has been widely recorded in the sub-tropical and temperate areas of the ocean (Carlson et al., 1994; Avril, 2002; Hansell and Carlson, 2001; Santinelli et al., 2013). The results of these studies indicate a lag between DOC sources and sinks, causing summer accumulation in the upper layers due to both biotic and abiotic processes, which either alter DOC bioavailability or reduce bacterial activity. Indeed, the inefficiency of the microbial loop in organic carbon mineralization – the so-called malfunctioning microbial loop (Thingstad et al., 1997) – induces an accumulation of bioavailable DOC. This inefficiency is directly related to low phosphate availability in the upper waters of the Mediterranean Sea (Moutin and Raimbault, 2002; Van Wambeke et al., 2002; Thingstad et al., 2005; Santinelli et al., 2013).

The pathway of organic carbon not only allows to estimate the total amount of fixed carbon, but it is also crucial to determining biological pump efficiency. Modeling was chosen to adress this question, taking into account the high heterogeneity of situations

New insights into the organic carbon export in the Mediterranean Sea from 3-D modeling

A. Guyennon et al.

Printer-friendly Version

Interactive Discussion

encountered in the Mediterranean Sea. In line with these considerations, the biogeochemical model was designed to be potentially efficient in every region (see Sect. 2). Major work has been done to estimate organic carbon export using box models (e.g. Toggweiler et al., 2003), ocean carbon-cycle models (e.g. Bopp et al., 2001; Sarmiento et al., 1998; Maier-Reimer et al., 1996; Sarmiento and Gruber, 2006) and ecosystem models coupled with hydrodynamic models (e.g. Le Quéré et al., 2010). The objective of this paper is to fit within this framework, but at a regional scale and at high resolution, with detailed description of biological processes. Several coupled models have also been developed to study the whole Mediterranean Sea, starting with the early simulation by Crispi et al. (1998); Crise et al. (1998). The number of models for this purpose is increasing (Lazzari et al., 2013; Macías et al., 2014; Mattia et al., 2013), but to our knowledge, no work has yet focused on organic carbon fluxes for the entire Mediterranean Sea. Moreover, the biogeochemical model Eco3M-MED is the only one able to analyze biogeochemical fluxes and stocks in the light of intracellular contents of planktonic organisms. In this paper, we aim to further investigate organic carbon export in the Mediterranean Sea in order to quantify the associated fluxes, to study their temporal and spatial variabilities, and to provide the first estimations at this scale of the respective contributions of DOC and POC to carbon export. To achieve this objective, we undertook 3-D biogeochemical modeling of the Mediterranean Sea using the biogeochemical model Eco3M-MED (Alekseenko et al., 2014), forced by physical simulations made with NEMO-MED12 (Beuvier et al., 2012b). The paper is organized as follows: in Sect. 2 a succinct overview of both models is given, given that they are fully detailed in the aforementioned papers. Simulation set-up and datasets used for model comparison are also presented. Sect. 3 first focuses on the assessment of the biogeochemical model outputs (nutrients, chlorophyll and primary production) through comparison with available data, then discusses results related to organic carbon inventory and export. In Sect. 4 results on export are examined in the context of previous POC and DOC export evaluations in the Mediterranean Sea.

2 Material and methods

2.1 The hydrodynamical model

The physical simulation used in this work was described by Beuvier et al. (2012b). The model used is the regional circulation model NEMOMED12 Beuvier et al. (2012a) which is part of a suite of Mediterranean regional versions of OPA and NEMO (Madec and The-NEMO-Team, 2008) as OPAMED16 (Béranger et al., 2005), OPAMED8 (Somot et al., 2006) and NEMO-MED8 (Beuvier et al., 2010).

Model resolution is $1/12°$ (≈ 8 km) which means that most of mesoscale features are explicitly resolved, and the domain includes the whole Mediterranean Sea as well as the Atlantic Ocean West of $11°$ W (Fig. 2). More details of the model and its parametrization are given in Beuvier et al. (2012a). The domain configuration and model have already been used to study Western Deep Water Formation (Beuvier et al., 2012a), sensitivity test to atmospheric forcings resolution (Lebeaupin Brossier et al., 2011), transport across the Strait of Gibraltar (Soto-Navarro et al., 2014) and anthropogenic carbon stocks evaluation (Palmiéri et al., 2015).

The simulation is initiated in October 1958 with temperature and salinity data representative of the 1955–1965 period using the MEDATLAS dataset (MEDAR/MEDATLAS-Group 2002; Rixen et al., 2005). Atmosphere forcings are applied daily and come from the ARPERA dataset (Herrmann et al., 2008), a 55 year simulation at 50 km and daily resolutions. SST-relaxation and water-flux correction terms, as well as fresh water input from rivers and the Black Sea and Atlantic exchanges are the same as described in Beuvier et al. (2010, 2012a).

2.2 The biogeochemical model

The biogeochemical model Eco3M-MED is embedded in the Eco3M modular numerical tool (Baklouti et al., 2006b), and its structure is similar to the model presented in Alekseenko et al. (2014). Figure 1 summarizes the interactions between the state variables

through the biogeochemical processes. We chose to represent three different element cycles C, N and P allowing to reproduce the different limitations and co-limitations observed in the Mediterranean Sea. Silicium, potentially limiting in some regions (Leblanc et al., 2003) is not represented in the model, as P and N limitations are the most com-
5   mon ones in the Mediterranean Sea. Six different planktonic functional types (P.F.T., see Le Quéré et al., 2005, for a proper definition) are represented: 2 primary producers (phytoplankton), 1 decomposer (heterotrophic bacteria) and 3 consumers (nano-, micro- and meso-zooplanktons). The structure of the trophic web thereby includes the main P.F.T.s of the Mediterranean Sea (Siokou-Frangou et al., 2010).
10   Every P.F.T. is represented in terms of biomasses (C, N, P, and Chlorophyll for producers) and abundances (cells per unit volume), except for meso-zooplankton which is only represented through its C biomass and its abundance (individuals per unit volume). The producers are split into two different P.F.T.s according to their theorical size, i.e. large phytoplankton ($> 10\,\mu m$) mainly encompassing diatoms, and small phyto-
15   plankton ($< 10\,\mu m$) which includes picophytoplankton and the remaining nanophytoplankton. The two P.F.T.s have different parameters (e.g. maximal growth rate, maximal uptake rate and affinity), distinct predators and they fuel different detritic pools (Fig. 1). Decomposers are represented by heterotrophic bacteria and are responsible for the organic matter mineralization, including hydrolysis of particles. Zooplankton is divided
20   into three different size groups, heterotrophic nanoflagellate (HNF) which feeds on bacteria and small phytoplankton, ciliate which feeds on small phytoplankton and HNF, and mesozooplankton (copepods) which feeds on ciliate, HNF and large phytoplankton. Copepods are the only metazoans of the model, and mechanisms such as individual growth, egg productions or reproduction are implicitly represented (Alekseenko et al.,
25   2014).
    Eleven processes are modeled: photosynthesis, chlorophyll production, respiration, mortality, growth, uptake, grazing, excretion, exudation, nitrification and particule hydrolysis. The formulations follow cell level mechanistic considerations, and intracellular concentrations, quotas and ratios are explicitly calculated. Detais are extensively

given in Baklouti et al. (2006a, 2011) and Alekseenko et al. (2014). Intracellular ratios and intracellular quotas are used to regulate growth via Droop's quota function (Droop, 1968) and net uptake and grazing rates via Geider's limitation formulation (Geider et al., 1998). Grazing, primary production and uptake rates are controlled firstly by the organism environment (either preys or nutrient concentration, or light availibility). Secondly, the internal cell status drives a feedback regulation of the net incorporated biomass. The uptaken extra is either released in its initial form or exuded in the form of DOM. The same assumptions are applied to estimate excretion (ammonium, phosphate), and fecal pellets production. Furthermore, 10 % of material grazed by mesozooplankton directly fuels the particulate organic matter stock, to represent sloppy feeding. Respiration rates are estimated via energy costs for every plankton activity (Alekseenko et al., 2014). Nitrification is represented through first order kinetics while particulate hydrolysis function depends on bacteria intracellular quotas (POC hydrolysis increases with bacterial C-limitation). Grazing by higher trophic levels is implicitely taken into account via a quadratic mortality affecting only mesozooplankton. Grazing function is a Holling II type (Holling, 1959; Kooijman, 2000) for multiple preys. The only difference with Alekseenko et al. (2014) configuration lies in the formulation used to represent predator preferences for multiple preys. We here used the "Kill The Winner" (KTW) formulation depicted in Vallina et al. (2014) which combines active-switching (i.e. the preference of a predator for a given prey depends on prey density) and an ingestion rate always increasing with the total biomass of preys. This active-switching formulation was used to preserve foodweb diversity (e.g Prowe et al., 2012) and to prevent unrealistic predator-prey oscillations.

Since the model relies on mechanistic basis, parameters are mainly physiological (and measurable) and they were either taken from literature or derived from other parameters on the basis of greater consistency between parameters.

2.3 Model coupling

The models NEMO and Eco3M-MED have been associated for the first time. The coupling between the hydrodynamic and biogeochemical models is offline, i.e. biological retroaction on physics is not taken into account. Daily-averaged water velocities were used for the advection of biogeochemical tracers, using a MUSCL scheme (lateral and vertical diffusions are calculated according to a centered scheme). The time-step used for the numerical integration of the tracer conservation equations equals 1200 s. A sinking velocity of $2\,m\,d^{-1}$ is applied only on the particulate organic pool (i.e. the detrital compartment). This compartment aims at representing particles with different sizes and sinking velocities and the value of $2\,m\,d^{-1}$ is within the usual range found in litterature (Vichi et al., 2007; Fasham et al., 2006). Light attenuation in the water column is modeled via the formulation of Morel (1988).

2.4 Initial and boundary biogeochemical conditions

Initial nutrient and chlorophyll fields are derived from annual means of the Mediterranean Sea climatology (Schaap and Lowry, 2010). The remaining biogeochemical variables are derived from chlorophyll using conversion factors derived from published works (see Alekseenko et al., 2014, for details).

A "buffer-zone" has been defined between the domain western boundary and the Gibraltar Strait (from 11 to 6° W), in which a damping procedure towards the Atlantic conditions has been applied. The restoring time is 2 days West of 7.5° W, lineary increasing to 90 days from 7.5 to 6° W (Fig. 2). Atlantic nutrient concentrations come from the World Ocean Atlas monthly climatology (Garcia et al., 2006), so that the nutrients damping in the "buffer-zone" takes into account the nutrients monthly variability. Given the imprecisions in phosphate measurements, we decided to compute phosphate profiles from that of nitrate by imposing a redfield ratio of 16 to be more coherent with observed $NO_3 : PO_4$ ratios in this region (Gómez, 2003). Chlorophyll concentrations were not provided in this database. We therefore used in situ data from the Sea-

DataNet database to create a mean vertical chlorophyll profile for the Atlantic, and then used a climatology of surface chlorophyll from the GlobColour product in this region to represent an annual cycle of the chlorophyll vertical profile. The remaining Atlantic biogeochemical variables were derived from chlorophyll using the same procedure as for initial conditions.

Nutrient (NO_3 and PO_4) inputs from riverine influx and coastal runoffs are derived from Ludwig et al. (2009), following the same procedure as for the riverine freshwater inputs in the circulation model (Beuvier et al., 2010, 2012b). The nutrient influx of the 29 rivers included in the RivDis database (Vörösmarty et al., 1996) are taken into account in the simulation, while the nutrients of the remaining rivers from Ludwig et al. (2009) database are averaged for every sub-basin and distributed along their respective sub-basin's coast as coastal runoffs. Dissolved organic carbon inputs in the Mediterranean Sea are distributed in every sub-Basin according to the riverine DOC estimates of Ludwig (1996) (a total of $\sim 2.1\,\mathrm{Tg\,C\,y^{-1}}$ in the whole Mediterranean Sea). Sub-Basin DOC inputs were then distributed among fluvial estuarines and coastal runoffs to match circulation model freshwater geographical distribution (Palmiéri, 2014; Palmiéri et al., 2015).

Mass exchanges with the Black Sea at the Dardanelles Strait are treated as river inputs, with nutrients and DOC input concentrations provided by the SESAME project (Tugrul and Besiktepe, 2007; Meador et al., 2010). But, since NO_3 budget indicates a negative net flux of NO_3 the Dardanelles Strait (i.e. exiting from the Mediterranean), NO_3 flux at Dardanelles is set to zero and the outcome is transferred on the Aegean sub-basin's runoffs. These runoffs are artificially reduced in order to keep the riverine budget of NO_3 in the Aegean sub-basin realistic.

2.5 Simulation set-up

Using the biogeochemical initial conditions defined in Sect. 2.4, we have conducted a 5 years simulation using physical forcings from the years 1973–1977. This first simulation was considered as a "spin-up", in order to reduce the impact of state variables

adjustment in the simulations. We used the final biogeochemical state of this spin-up as initial conditions for a second simulation running from 1996 to 2012. In this simulation, only the years following 1998 are considered, since the first 3 years were treated as an additional spin-up.

2.6 Data description

The present work intends to study and to quantify organic carbon export fluxes with a 3-D physical-biogeochemical model. For this purpose, our first objective was to assess the reliability of our model by examining the agreement between different model outputs and corresponding available data: chlorophyll, nutrients, DOC concentrations and primary production rates.

Three type of comparisons were undertaken:

  i. at basin scale, using surface chlorophyll fields provided by satellite for comparisons at different seasons

  ii. at basin scale, using BOUM cruise transect as a "snapshot" to compare nutrients vertical profiles

  iii. at a local scale using the time series data collected at DyFaMed station

2.6.1 Chlorophyll data derived from satellite

Among the specificities of the Mediterranean Sea, its strong oligotrophy and the major influence of colored dissolved organic matter, make the use of classical satellite chlorophyll products difficult (e.g. Claustre et al., 2002). Several algorithms have already been developped (Bosc et al., 2004; D'Ortenzio et al., 2002; Volpe et al., 2007), using different satellite reflectances and datasets. Here, we used a daily surface chlorophyll product delivered by the Myocean project (http://www.myocean.eu). In this product, chorophyll concentrations have been derived using the MEDOC4 algorithm developped by Volpe et al. (2007) and applied to multi-sensor marines reflectance produced

in the frame of the Climate Change Initiative of the European Spatial Agency (CCI-ESA http://www.esa-oceancolour-cci.org/). This algorithm has been built using a large dataset of in situ chlorophyll concentrations collected and reflectance measurements from 3 satellites (Seawifs, MERIS and MODIS), constituting an homogeneous serie from September 1997 to March 2012. Daily chlorophyll maps are then aggregated into eight-days maps (i.e. 46 per year) to reduce data gaps. Besides, a spatial smoothing operator is applied on 5 pixel squares (≈ 40 km) with distance-derived weights to reduce spatial noise.

2.6.2 The BOUM cruise data

The BOUM cruise took place during summer 2008 (from June 16 to July 20) and crossed both the Western and Eastern Basins of the Mediterranean Sea (Moutin et al., 2012). The data acquired during this cruise give a unique picture of the biogeochemical status of the Mediterranean Sea during a stratified period since many biogeochemical variables have been observed. Measurements of nutrients concentrations were used to perform a Basin-scale observation with the corresponding model outputs.

2.6.3 The DyFaMed station data

The DyFaMed station is located in the Ligurian Sea at 7.9° E and 43.4° N, 50 km off Cap-Ferrat (Fig. 2) and is isolated from coastal inputs by the Mediterranean Northern Current. A strong winter mixing is observed in this area, although less intense than the deep convection occuring in the Provencal sub-Basin (Marshall and Schott, 1999). Nutrients, chlorophyll, dissolved organic carbon time series were used for comparison.

The comparison of the model outputs with DyFaMed time series can be done through different methods. The simplest one consists in using a single grid point which is the nearest from the DyFaMed station location. This implies that the model perfectly reproduces spatial patterns in this region, which is obviously never the case. On the other hand, the use of model outputs averaged on several grid points around DyFaMed

New insights into the organic carbon export in the Mediterranean Sea from 3-D modeling

A. Guyennon et al.

Title Page

Abstract | Introduction

Conclusions | References

Tables | Figures

◄ | ►

◄ | ►

Back | Close

Full Screen / Esc

Printer-friendly Version

Interactive Discussion

station amounts to dampening signal variability. We finally chose to use the nearest gridpoint to DyFaMed station, while assessing spatial variability in the 8 neighbouring grid points (Table 2).

3   Results

3.1   Model skill assessment

For reasons of brevity, model outputs hereafter have the prefix "m" while corresponding in situ or satellite observations have the prefix "o".

3.1.1   Nutrients

Basin scale spatial variability

Along the BOUM transect, mNO_3 varies between 0.12 and 7.8 µmol L^{-1} in the Western Basin, and between 0.36 and 5.7 µmol L^{-1} in the Eastern Basin (Fig. 3). mPO_4 varies between 0 and 0.34 µmol L^{-1} in the Western Basin, and between 0 and 0.18 µmol L^{-1} in the Eastern Basin (Fig. 4). Corresponding ranges from BOUM data are wider (higher maxima) for both nitrate and phosphate, as summarized in Table 1.

In the surface layer (0–30 m), mNO_3 is less than 1 µmol L^{-1}, with a mean value of around 0.5 µmol L^{-1} for the whole Basin, while mPO_4 is almost nil everywhere (< 0.01 µmol L^{-1}). These values are consistent with measured nutrient concentrations, which are low and close to their quantification limits of 0.05 µmol L^{-1} for both NO_3 and PO_4 (Figs. 3, 4 and Table 1). Modeled nutrient concentrations increase with depth and remain at their maximum values from the bottom of the nutriclines to the bottom of the sea. Western Basin average deep mNO_3 and mPO_4 are 7.7 and 0.34 µmol L^{-1}, respectively, and Eastern Basin average values are 5.4 and 0.15 µmol L^{-1} respectively (Table 1). When compared to in situ data, average mNO_3 [mPO_4 in brackets] is un-

derestimated by 1.2 [0.04] µmol L^{-1} in the Western Basin, and 0.4 [0.01] µmol L^{-1} in the Eastern Basin. The modeled top nitracline is located at around 30 m depth along the entire BOUM transect. The top phosphacline depth ranges between 50 and 120 m with a mean of about 80 m, except in the South Ionian Sea, where it ranges between

5 120 and 160 m (Figs. 3 and 4). In the Western Basin, the top of the modeled nitracline is almost 25 m over the top nitracline derived from in situ data, and the gap increases eastward as the top nitracline derived from data gets deeper (Moutin and Prieur, 2012). The modeled top phosphacline is also below the data-derived top phosphacline. The difference between model outputs and data can also be found in the slope of the nitr-

10 acline at depths of between 150 and 1000 m: this slope decreases with depth for the model, while it is quite constant for data. As a consequence, significant differences in nitrate concentration can be observed in the "intermediate" waters (between 250 and 1000 m): model mean concentrations are underestimated by almost 3 µmol L^{-1} at 500 m in the Western Basin, 1.5 µmol L^{-1} in the Ionian Basin and 1.2 µmol L^{-1} in the

15 Levantine Basin. In the Western Basin, the same differences between model and data were found in the phosphate vertical profiles (Fig. 4, Table 1), resulting in a maximum difference of 0.15 µmol L^{-1} in phosphate concentrations. However, in the Eastern Basin, modeled and in situ phosphate gradients are in better agreement than nitrate gradients, except that the phosphacline is less thick than in data, leading to an underestimation of

20 deep concentrations by the model. Deep mNO_3 and mPO_4 decrease from west to east along a well-described gradient, which is in agreement with observations (Pujo-Pay et al., 2011). The $mNO_3 : mPO_4$ ratio at 1500 m in the Western Basin ranges between 21 and 24 and is very close to the measured ratio, which lies between 22 and 23. In the Eastern Basin, the modeled ratio decreases eastward from 42 to 31, while the

25 measured ratio ranges between 27 and 31. In addition, some discrepancies between model and observations are attributable to the hydrodynamic model (e.g. mislocation of the anti-cyclonic eddies). Despite the aforementioned model weaknesses, modeled concentrations are in overall agreement with data.

Seasonal and vertical variabilities

At DyFaMed station, most of the spatial and temporal variabilities in nutrient concentrations are observed within the surface layer (see Figs. 5, 6 and Table 2). In the upper layer (0–30 m), mNO_3 and mPO_4 exhibit a seasonal pattern, with values regularly lower than $0.5 \, \mu mol \, L^{-1}$ from May (March for mPO_4) to October, increasing thereafter to reach a maximum in January ranging from 3.2 to 4.1 (0.03 to 0.07 for mPO_4) $\mu mol \, L^{-1}$ depending on the year.

This is very similar to the evolution of observed NO_3 which is also below $0.5 \, \mu mol \, L^{-1}$ from May to October and reach a maximum ranging from 2 to 6.4 $\mu mol \, L^{-1}$ in January–February. In summer, however, oNO_3 is often almost below the quantification limit while mNO_3 is never below $0.2 \, \mu mol \, L^{-1}$. oPO_4 is below the quantification limit in almost every observation made above 30 m depth, except between January and March where oPO_4 can reach 0.15 $\mu mol \, L^{-1}$. These maxima are underestimated by the model, as mPO_4 never exceeds $0.07 \, \mu mol \, L^{-1}$ (close to the quantification limit).

In both model outputs and observations, the highest values of surface PO_4 and NO_3 correspond to the period of winter mixing (down to 100 m depth) in January–February. The $1 \, \mu mol \, L^{-1}$ isoline of nitrate (see Fig. 5), which is a good indicator of the seasonal signal, has quite similar locations in the model and in data, lying at a maximum depth of around 40 m between March and October, and reaching the sea surface from November–December to March. For phosphate, the available observations show that the $0.1 \, \mu mol \, L^{-1}$ isoline reaches the surface during mixing, while the modeled isoline remains below 50 m depth.

Between 30 and 1000 m depth, observed and modeled NO_3 and PO_4 concentrations are consistent with each other though observations show higher mean values and larger ranges (see Table 2) quite systematically. The highest absolute differences along the water column are observed between 250 and 500 m depths for nitrate where mNO_3 is underestimated by $1.5 \, \mu mol \, L^{-1}$, and between 30 and 100 m for phosphate where the mean mPO_4 is very low ($< 0.02 \, \mu mol \, L^{-1}$) while oPO_4 equals $0.14 \, \mu mol \, L^{-1}$. It must be

reminded however that DyFaMed observations are compared to a single grid point of the modeled domain which is submitted to variability due to hydrodynamical features. We evaluated potential impact of variability by calculating the RMSD between 8 neighbouring grid points and the single grid point chosen. The impact of spatial variaibility is weak on temporal means (< 0.13 and $0.01\,\mu mol\,L^{-1}$ for NO_3 and PO_4 respectively) and stay below 0.5 and $0.04\,\mu mol\,L^{-1}$ during the whole period, and therefore cannot fully explain the differences observed.

3.1.2 Chlorophyll

Basin scale variability

Four distinct periods (winter, spring, summer, and autumn) have been chosen to present the variability of both satellite (oCHL) and model-derived (mCHL) chlorophyll concentration climatologies (Fig. 7). mCHL is calculated as the average concentration through the first 10 m of the water column for the 2002–2011 period. The contrast in mCHL between the Western and Eastern Basins is the highest during winter and spring, whereas it is marked throughout the year for oCHL. Excluding the coastal regions (depths lower than 190 m), median mCHL in the West [East in brackets] Basin is equal to 0.21 [0.06], 0.66 [0.09], 0.10 [0.11] and 0.12 [0.12] $\mu g\,L^{-1}$, respectively for winter, spring, summer, and autumn, while the corresponding values for the median oCHL is equal to 0.27 [0.08], 0.24 [0.07], 0.05 [0.03] and 0.10 [0.05] $\mu g\,L^{-1}$.

Moreover, year-long high chlorophyll clusters can be seen in both oCHL and mCHL close to the main river mouths (the Nile, Rhone, Po, Ebro or Tiber), and only in oCHL in the Dardanelles Strait, along the western coast of the Adriatic Sea and in the Gulf of Gabes. Apart from these permanent features, seasonal chlorophyll patterns are compared, as follows.

During winter (Fig. 7a and e), high surface chlorophyll values are modeled and observed in the Western Mediterranean, particularly in the Alboran Sea where mCHL and oCHL values range between 1 and 2.4 and between 0.2 and 0.6 $\mu g\,L^{-1}$, respec-

Title Page

Abstract | Introduction

Conclusions | References

Tables | Figures

|◄ | ►|

◄ | ►

Back | Close

Full Screen / Esc

Printer-friendly Version

Interactive Discussion

tively. The high oCHL in the Alboran Sea extends along the Algerian coast, a pattern not reproduced by the model. Elsewhere in the Western Basin, oCHL is less patchy than mCHL since the model reaches high values in the deep convection area and low concentrations in the Tyrrhenian Sea that are not observed on the satellite map. On the other hand, the local minimum around 42° N 5° E, where convection mixing is the most intense, is well-represented by the model. The Liguro-Provencal current associated with low concentrations is more clearly visible in mCHL than in oCHL ($mCHL < 0.1\,\mu g\,L^{-1}$). East of the Sicilian Strait, mCHL and oCHL values are mainly below $0.1\,\mu g\,L^{-1}$ when the Adriatic Sea is not taken into account. In the open sea, the most visible pattern is the Rhodes Gyre with chlorophyll values above $0.2\,\mu g\,L^{-1}$. In the Adriatic Sea, mCHL and oCHL are both close to $0.2\,\mu g\,L^{-1}$ (excluding the western coast) although mCHL is more patchy due to the presence of two structures with higher mCHL (from 0.3 to $0.6\,\mu g\,L^{-1}$).

During spring, the spatial pattern of oCHL (Fig. 7b) is less homogeneous than in winter. The mCHL pattern (Fig. 7f) is quite similar to the one modeled in winter, albeit with higher concentrations and sharper horizontal gradients. In the Western Basin, mCHL values range between 0.3 and $> 3\,\mu g\,L^{-1}$ and oCHL values range between 0.1 and $> 1\,\mu g\,L^{-1}$. In the Eastern Basin, excluding the Adriatic Sea and the already mentioned permanent hot spots, chlorophyll concentration are low (around $0.1\,\mu g\,L^{-1}$), particularly in the south. Modeled and satellite chlorophyll patterns show roughly the same main structures, namely (i) a well-marked Liguro-Provencal bloom, which is, nevertheless, more intense and more expanded in the model, (ii) a clearly visible northern current (NC), and (iii) a patch with high chlorophyll concentrations in the Rhodes Gyre. Two patches with high core CHL values ($> 1.2\,\mu g\,L^{-1}$) are simulated in the Adriatic Sea and not observed in oCHL.

During summer, mCHL (Fig. 7g) is quite homogeneous in the whole Mediterranean Basin and values are about $0.1\,\mu g\,L^{-1}$ with the exception of some minimum values ($< 0.05\,\mu g\,L^{-1}$) in the area from the Algerian coast to the Balearic Islands and within the anti-cyclonic Alboran eddies, and some maximum values ($> 0.5\,\mu g\,L^{-1}$) in the north-

western part of the Alboran Sea. oCHL values (Fig. 7c), are below mCHL values almost everywhere, at around $0.05\,\mu g\,L^{-1}$ with the exception of in the North-Western Alboran Sea where they are above $0.5\,\mu g\,L^{-1}$. The chlorophyll decrease in the Algerian Basin, the ending of the bloom in the Provencal sub-Basin and the Rhodes Gyre, and the low

5 concentrations in the Tyrrhenian Sea and Eastern Basin are well represented by the model. However, the eastward gradient of oligotrophy is not clearly visible in the model.

During autumn, the situation is close to that in summer, with mean mCHL values of $0.1\,\mu g\,L^{-1}$ (Fig. 7h). Local maxima ($0.15\,\mu g\,L^{-1}$) are, however, discernable in the Provencal sub-Basin, the Rhodes Gyre, the Eastern Corsica patch, and the region

10 between Sardinia and Sicily. Other local maxima with higher concentrations ($0.4\,\mu g\,L^{-1}$) are identified in the Alboran Sea, from the Gibraltar Strait to the cyclonic gyre located at 1° W. oCHL values are below $0.1\,\mu g\,L^{-1}$ in the whole Mediterranean Basin with the exception of along the Algerian coast, the Alboran Sea, the Provencal sub-Basin and the Adriatic Sea, where concentrations are higher but remain below $0.3\,\mu g\,L^{-1}$ (Fig. 7d).

15 The model is able to track the location and the seasonal dynamics of all the major productive areas detected by the satellite, namely the main river mouths, the North-Western Alboran Sea, the Rhodes Gyre and the Liguro-Provencal sub-Basin, excluding the Gulf of Gabes, where the shallow depth combined with high coastal supplies that are not introduced into the model render correct representation of this area very

20 difficult. On the contrary, the Adriatic Sea is highly productive in the model outputs, particularly within the two patches identified, but satellite observations do not support these findings. It is likely that a failure of the hydrodynamic model is responsible for this misrepresentation of the chlorophyll concentrations. During winter and spring (Fig. 7a, b, e and f), mCHL values generally tend to be higher than oCHL values and this is

25 particularly true in the Western Basin.

The mCHL variability is largely dominated by high values in the Alboran Sea as far as the Balearic Island (2° E), following the pattern of the numerous mesoscale physical structures that are simulated in this area. However, according to satellite measurements, high productivity in the Alboran Sea is limited to the region west of 3° W. Along

the Algerian coast, the high concentrations observed by satellite are not reproduced by the model.

Chlorophyll concentrations and spatial patterns are quite well reproduced by the model (Fig. 7), and this is also the case for some typical biogeochemical features of the Mediterranean Sea. For example, (i) the modeled spring bloom in the Provencal sub-Basin is well separated from the coast by the weakly productive Ligurian Northern Current, (ii) the partition between Western and Eastern Basins is visible eastward of the Sicilian Strait, (iii) the content of the Rhodes Gyre is higher than that of the Levantine.

The model values of the central Eastern Basin are within the range of observations, with maximum values of below $0.3\,\mu g\,L^{-1}$ (Fig. 7) in the open sea. However, minimum chlorophyll concentrations are obtained during spring by the model and this is in disagreement with observations. Models intercomparison is beyond the scope of this paper, however comparisons with former simulations (Lazzari et al., 2012; Mattia et al., 2013) can give some informations. It is noteworthy that results from Mattia et al. (2013) showed a more important bias in the Eastern Basin than in the Western Basin, with higher annual concentrations compared to satellite measurements. The maximum of surface chlorophyll in the Eastern Basin was simulated in winter (as for satellite chlorophyll) in Mattia et al. (2013). This is also the case in the simulation runned by Lazzari et al. (2012), however summer concentrations seemed to be underestimated in that case.

Seasonal surface variability

Timing of chlorophyll seasonal variations is satisfactorily reproduced by the model when regarding the Provencal sub-Basin, the Tyrrhenian Sea and the Rhodes Gyre (Fig. 7). To further study the seasonal variability of surface chorophyll, we used (for the satellite and model-derived chlorophyll concentrations) the metric ΔChl defined as

Full Screen / Esc

Printer-friendly Version

Interactive Discussion

follows:

$$\Delta Chl = \frac{\max(Chl_{year})}{median(Chl_{year})} \quad\quad (1)$$

High values of ΔChl can therefore be related to a strong seasonal variability, while low values, typically < 2, can be associated with a constant signal (Fig. 8).

For both model and satellite, the seasonal signal is particurarily important in the Liguro-Provencal sub-bassin (ΔChl > 10) and the Algerian Coast (ΔChl$_{sat}$ about 8, ΔChl$_{mod}$ above 10). ΔChl is broadly above 6 for model and 4 for satellite in the Western Basin west of 9° W. In the Tyrrhenian Sea, ΔChl is close to zero for the model, except for the area along the Italian Coast, while ΔChl for satellite is above 3 with a maximum value around 6.

In the Eastern Basin, model ΔChl is almost nil everywhere except in the Rhodes Gyre (> 10) and in the Adriatic Sea where two patches of values above 10 can be seen. This is consistent with oCHL values which are also low, except in the south Levantine Basin (about 2), in the Rhodes Gyre (> 6) and in the Gulf of Gabes (> 6). In the Adriatic sea, a patch of values of ΔChl above 3 is visible in the South.

Using SeaWiFS and MODIS surface chlorophyll data from 1998 to 2010 and the statistical work from D'Ortenzio and Ribera d'Alcalà (2009); Lavigne et al. (2013) identified 9 different regions on the basis of the seasonality of the chlorophyll signal. These regions are consistent with the ones emerging from the present study. The North-West bloom region is associated with the region of the highest values of ΔChl$_{mod}$ and ΔChl$_{sat}$. The Algerian region is characterized by relatively high ΔChl values, while the intermittent Rhodes Gyre region is identified as highly variable in the present study according to satellite data and model outputs. The distinction between the South and North Ionian Basins in the bioregionalization, also visible satellite ΔChl is absent in the model ΔChl.

Vertical and temporal variabilities

At the DyFaMed station, a strong seasonal variability in chlorophyll concentrations can be observed in both model outputs and in situ data (Marty et al., 2002; Marty and Chiavérini, 2010). Chlorophyll data (oCHL) and modeled ones (mCHL) are consistent with each other as shown in Fig. 9: they both show a bloom occurring in late February early March, after the period of maximum mixing (mid February in this area), characterized by high chlorophyll concentrations inside the mixing layer (down to 150 m depth). A second less intense and shallower bloom often follows in April, characterized by chlorophyll concentrations above $1.5\,\mu g\,L^{-1}$ in both model outputs and observations.

Following April, a Deep Chlorophyll Maximum (DCM) is visible in both observations and model: the patch of high mChl ($> 1.5\,\mu g\,L^{-1}$) deepens and the DCM settles down to ≈ 30 m depth with values about $0.2\,\mu g\,L^{-1}$, while oCHL DCM deepens to 50 m and its intensity slowly decreases down to concentrations around $1\,\mu g\,L^{-1}$.

During summer, surface concentrations are at their lowest level with values of mChl and oChl often below $0.1\,\mu g\,L^{-1}$. As the mixing layer depth gradually increases in autumn, mChl surface values first increase by dilution of the DCM (vertically integrated chlorophyll remains constant) and then decreases until the restart of primary production in early February. These results are consistent with the oCHL pattern.

Surface chlorophyll is well reproduced by the model with a maximum observed in early spring and very low concentrations from June to October. Concerning the modeled DCM (Fig. 9, top), it is shallower than the one derived from observations. However, when looking at the two chlorophyll contributors of the model, it appears that the DCM associated with large phytoplankton is close to the observed one. This means that the difference in the DCM depth is likely due to the underestimation of large phytoplankton concentrations at depth by the model during summer (see also Sect. 4.1).

3.1.3 Primary production

In the following section, mIPP refers to the modeled integrated Gross Primary Production, i.e. to the total amount of inorganic carbon fixed by the two phytoplankton groups integrated over the water column. The equivalent for observations will be referred to as
5 oIPP.

Spatial variability

The mean annual mIPP of the whole Basin over the 2000–2012 period equals 82 $\mathrm{g\,C\,m^{-2}\,y^{-1}}$, which is in the range of published values: 98 (Lazzari et al., 2012), 80–90 (Sournia, 1973), 68 (Uitz et al., 2012), 136 (Bosc et al., 2004) or 156 (Antoine et al.,
10 1995) using a coupled model, a climatology of ^{14}C measurements, and satellite-derived production in the last three references, respectively. mIPP values in the Mediterranean Sea range between 35.4 and 270 $\mathrm{g\,C\,m^{-2}\,y^{-1}}$, showing a strong spatial heterogeneity (see Fig. 10a).

A gradient in mIPP is observed from west to east: the Western Basin production is
15 almost twice that of the Eastern Basin, which is coherent with the dissimilarity in chlorophyll and nutrients already mentioned. This ratio is coherent with the oIPP derived from in situ measurements (Moutin and Raimbault, 2002), but higher than that found using the satellite or models (Uitz et al., 2012; Bosc et al., 2004; Lazzari et al., 2012).

In what follows, mIPP is compared to the oIPP derived from satellite data by Bosc
20 et al. (2004) and Uitz et al. (2012). These studies both show quite similar oIPP spatial distributions despite the two analyses having been conducted during different periods (1997–2001 for Bosc et al., 2004 and 1998–2007 for Uitz et al., 2012). IPP calculated by Bosc et al. (2004) tend to overestimate observations, particularly in ultra-oligotrophic regions, but IPP from Uitz et al. (2012) does not show a trend of error. In the different
25 regions defined in Bosc et al. (2004), mIPP is mostly within the range defined by the two studies. More importantly, the hierarchy in term of IPP between different regions is similar between model and satellite products. In the Western Basin, the level of pro-

Title Page

Abstract | Introduction

Conclusions | References

Tables | Figures

◄ | ►

◄ | ►

Back | Close

Full Screen / Esc

Printer-friendly Version

Interactive Discussion

ductivity of the different regions is the same, with the exception of the Algero-Provencal Basin which is the less productive in both satellite products (Table 3).

Small phytoplankton (including pico- and nano-phytoplankton) are by far the main contributor to mIPP (Fig. 10b) at the Mediterranean scale (78 %).

This is particularly true across the Eastern Basin, where the mean contribution of large phytoplankton is less than 5 %. Large phytoplankton contribution is almost nil in the Levantine and Ionian Basins, and only the Rhodes Gyre shows a significant activity of large phytoplankton. In the Adriatic Sea, large phytoplankton contribution to mIPP is almost 50 %.

In the Western Basin, small phytoplankton still dominates mIPP (62 %), with the exception of in the two most productive regions (Alboran Sea and Liguro-Provencal sub-Basins) where mIPP can be principally attributed to large phytoplankton. The predominance of small organisms is typical of the Mediterranean Sea and, more broadly, of the oligotrophic areas (see reviews by Siokou-Frangou et al., 2010; Magazzu and Decembrini, 1995). Picophytoplankton may account for 65 % of the primary production (Siokou-Frangou et al., 2010), with a wide range of proportions from 31 to 92 %, and particularly high proportions in the Eastern Basin. The contribution of large phytoplankton to primary production can be significant in regions associated with higher hydrodynamic variability such as the Alboran gyres, the Rhodes Gyre or sites of deep water formation (Ligurian and South Adriatic Seas, Siokou-Frangou et al., 2010).

Seasonal variability

In addition to satellite data, in situ oIPP measured at the DyFaMed station between 1991 and 1999 (Marty and Chiavérini, 2002) were used for comparison with mIPP (Fig. 11). Since in situ data and simulations cover different periods of time, we compared mean seasonal variations only. The model and observations show very similar patterns, with a maximum in March–April, and a slight decrease from July to December. Most daily measurements of primary production are within the interannual range of modeled values.

3.2 Organic carbon inventory and export

3.2.1 Dissolved organic carbon inventory

In what follows, mDOC refers to the modeled dissolved organic carbon integrated over the first 100 m of the water column. Seasonal variations of mDOC are given in Fig. 12.
Low mDOC values ($< 1 \, \text{mol m}^{-2}$) are observed throughout the year in the region extending from the Gibraltar Strait to the Balearic Islands, and in some well marked patches between Corsica and Sicilia Islands, and East of the strait of Bonifacio. On the opposite, very high mDOC values ($> 5 \, \text{mol m}^{-2}$) can be found in the North Adriatic Sea and along the Lybian Coast. During winter (Fig. 12a), mDOC remains below $2 \, \text{mol m}^{-2}$ except for the regions mentioned above. Local mDOC minima are observed in the North-Eastern Basin, especially in the Rhodes Gyre but also in the South Adriatic Sea and in the Provencal sub-Basin. During spring (Fig. 12b), relatively high mDOC values are observed in the Liguro-Provencal sub-Basin ($> 3 \, \text{mol m}^{-2}$) and in the Adriatic Sea ($> 4 \, \text{mol m}^{-2}$). During summer (Fig. 12c), mDOC in the Western Basin is mainly above $3 \, \text{mol m}^{-2}$ with values reaching $4 \, \text{mol m}^{-2}$ in its central part. Values are lower (about $2 \, \text{mol m}^{-2}$) in the Tyrrhenian Sea. In the Eastern Basin, mDOC values reach $2 \, \text{mol m}^{-2}$ in the Ionian Basin, and increase southward to reach $3 \, \text{mol m}^{-2}$ along the Libyan Coast. Along the Eastern coast of the Levantine Basin, high values ($> 5 \, \text{mol m}^{-2}$) are obtained. During autumn (Fig. 12d), mDOC values are high in almost every coastal areas. In the whole Basin, mDOC is higher than $2.5 \, \text{mol m}^{-2}$, except in the central Levantine Basin where it is below $2 \, \text{mol m}^{-2}$.

The highest mDOC seasonal variations are observed in coastal areas and in the South Ionian Sea. Elsewhere, mDOC variations are high in the whole Ionian Sea, the Tyrrhenian Sea, the North Adriatic Sea, the Provencal sub-Basin and the Algerian sub-Basin. The highest DOC concentrations are generally observed in summer in the Western Basin and the Adriatic Sea, and in autumn in coastal areas and in the South Ionian Sea.

Regular measurements of total DOC (i.e. including refractory and semi-refractory pools) performed at DyFaMed site (Avril, 2002) were used for comparison. Since the model only provides the labile and semi-labile DOC pools, the in situ DOC concentration measured in deep water ($> 1000\,\mathrm{m}$), which can be considered as refractory DOC, has been added to the model DOC output. Moreover, since our run does not cover the period of in situ data, we decided to work on a climatology of DOC vertical profiles: bi-monthly mean, maximal and minimal DOC values were calculated and compared (Fig. 13).

The climatology of DOC at DyFaMed proposed by Avril (2002) is divided into three periods. During spring, DOC stocks increase just after the bloom and DOC is related to the POC hydrolysis at depth. During summer, stratification isolates the surface layer where DOC accumulates due to the activity of small phytoplankton and to reduced bacterial activity. Then, during winter the water column is mixed. At the DyFaMed grid point, model outputs also show a DOC increase during spring (April–May), but close to the surface. Then, in summer, the DOC production rate is lower than in spring but still significant and limited to the upper layers. Surface DOC stocks decrease (as of September) with mixing. DOC seasonal variations of both the model and observations are maximal at surface, however modeled DOC variations rapidly decrease with depth and they are lower than observations at $150\,\mathrm{m}$ depth.

As a consequence, the modeled DOC vertical gradient is higher than the observed one, particularly in summer. DOC stocks variations are higher in the model: integrated DOC within the first $100\,\mathrm{m}$ ranges between 5.5 and $9.4\,\mathrm{mol\,m^{-2}}$ for the model, and between 7.2 and $8.7\,\mathrm{mol\,m^{-2}}$ for in situ data.

3.2.2 Particulate organic carbon inventory

During winter (Fig. 14a), the highest values of mPOC ($> 0.5\,\mathrm{mol\,m^{-2}}$) are found in the region of the Alboran Sea and the surrounding Balearic Islands. A patch of values around $0.3\,\mathrm{mol\,m^{-2}}$ is observed in the Provencal sub-Basin. In the Adriatic Sea, mPOC is in the range $[0.1;0.2]\,\mathrm{mol\,m^{-2}}$. Elsewhere, mPOC is very low ($< 0.1\,\mathrm{mol\,m^{-2}}$). During

spring (Fig. 14b), the maximum mPOC is observed in the Provencal sub-Basin and the North Adriatic Sea. In the Western Basin, mPOC is higher than $0.2\,\mathrm{mol\,m^{-2}}$ and reach $0.4\,\mathrm{mol\,m^{-2}}$ in the Alboran Sea, except in the Tyrrhenian Sea where it remains below $0.05\,\mathrm{mol\,m^{-2}}$. In the Eastern Basin, values of mPOC are generally below $0.05\,\mathrm{mol\,m^{-2}}$, although in the Rhodes Gyre, values up to $0.15\,\mathrm{mol\,m^{-2}}$ are calculated. Values from 0.2 to $0.5\,\mathrm{mol\,m^{-2}}$ are obtained in the whole Adriatic Sea. During summer (Fig. 14c), overall values are low ($< 0.05\,\mathrm{mol\,m^{-2}}$), except in the Alboran Sea where values reach $0.2\,\mathrm{mol\,m^{-2}}$ and in the North Adriatic Sea. During autumn (Fig. 14d), the patterns are close to the ones in summer except that values are slighlty higher (about $0.3\,\mathrm{mol\,m^{-2}}$) in the Alboran Sea.

Some major differences in the integrated POC seasonal signal exist between basins. In the Eastern Basin, mPOC remains low ($< 0.05\,\mathrm{mol\,m^{-2}}$) all over the year, except for local maxima in the Rhodes Gyre distinguishable in spring (May–June). mPOC seasonal variations are limited to the Western Basin and the Adriatic Sea, especially in the Alboran Sea and the deep convection area (Liguro-Provencal Basin). In the latter, mPOC declines almost towards zero in summer, and starts increasing in late winter (March). The dynamics in the Adriatic Sea is quite similar, except in the North where a maximum mPOC is calculated in summer. In the Western Alboran Sea (West 0°), mean mPOC remains above zero all over the year: it starts increasing in early winter (January) and remains relatively high until the summer decrease.

3.2.3 Dissolved and particulate organic carbon export

Spatial variability

Organic carbon fluxes are computed at 100 and 200 m by adding the contribution of advection (vertical velocity and settling velocity for POC) and diffusion (implicitly representing turbulence and convection mixing) processes across the grid. Negative fluxes account for downward fluxes. For clarity fluxes will be referred to as F_{DOC}, F_{POC} and F_{OC} as the sum of the two latter. Mean F_{OC} over the whole basin equals $-22.8\,\mathrm{g\,C\,m^{-2}\,y^{-1}}$

(median of $-17.8\,\mathrm{g\,C\,m^{-2}\,y^{-1}}$). 95 % of the flux values are within the range -80 to $12\,\mathrm{g\,C\,m^{-2}\,y^{-1}}$ with extreme values indicating a large spatial variability. According to the model, the main regions of organic carbon export are the Liguro-Provencal sub-Basins, the Alboran Sea, the southern continental slopes and the Adriatic Sea.

5   DOC contribution to the total organic carbon flux is dominant (Fig. 15). In the Western Basin, the global amounts of exported POC and DOC below 100 m are respectively $7.0\,\mathrm{Mt\,C\,y^{-1}}$ and $12.7\,\mathrm{Mt\,C\,y^{-1}}$, meaning that 64 % of this export is due to DOC. In the Eastern Basin, DOC is responsible of 90 % of the organic carbon export below 100 m, with an annual flux of 26.1 (against 2.6 for POC) $\mathrm{Mt\,C\,y^{-1}}$. DOC export occurs in both
10 Western and Eastern Basins in relative similar proportion compared to POC export.

In the Western Basin, 95 % of downward F_{DOC} values range from 1 to $69\,\mathrm{g\,C\,m^{-2}\,y^{-1}}$ with a stronger variability within coastal and shallow areas. High positive values (i.e. upward) of F_{DOC} are simulated along the French and Spanish Coasts, the entrance of the Sicilian Strait and North-East of Corsica. Excluding these areas, the highest
15 downward fluxes of DOC, highlighted by the black contours in Fig. 15 top, are calculated in the Provencal sub-Basin (especially in the region of deep convection), the North of the Balearic Islands and along the Algerian slope, where downward F_{DOC} can be higher than $60\,\mathrm{g\,C\,m^{-2}\,y^{-1}}$. In the Algerian Basin, the Balearic Sea and the Tyrrhenian Sea, F_{DOC} values are quite homogeneous and range from -5 to $-15\,\mathrm{g\,C\,m^{-2}\,y^{-1}}$.

20 In the Eastern Basin, 95 % of the downward F_{DOC} values range from 4 to $74\,\mathrm{g\,C\,m^{-2}\,y^{-1}}$. The complexity of topography and hydrodynamical regimes in the Aegan Sea may explain the high heterogeneity of the fluxes calculated in this region that are difficult to interpret. Highest downward F_{DOC} values are located along the continental slopes from the Lybian to the Turkish Coasts and in the Adriatic Sea where the
25 median value is around $-25\,\mathrm{g\,C\,m^{-2}\,y^{-1}}$. F_{DOC} is more homogeneous in the open sea, with a median of $-17\,\mathrm{g\,C\,m^{-2}\,y^{-1}}$.

A strong difference exists between the Western and Eastern Basins regarding F_{POC} at 100 m. Mean value of downward F_{POC} over the Western Basin is $-9.8\,\mathrm{g\,C\,m^{-2}\,y^{-1}}$

(median of $-7.8\,\mathrm{g\,C\,m^{-2}\,y^{-1}}$) and $-2.4\,\mathrm{g\,C\,m^{-2}\,y^{-1}}$ (median of $-1.9\,\mathrm{g\,C\,m^{-2}\,y^{-1}}$) in the Eastern Basin (Fig. 15, bottom).

In the Western Basin, F_{DOC} is the highest (see black contour in Fig. 15, bottom), in the Alboran Sea, particularly in the South East of the easily identifiable anticyclonic eddies. Following the pathway of the Atlantic waters, downward F_{POC} values decrease to reach absolute values lower than $5\,\mathrm{g\,C\,m^{-2}\,y^{-1}}$ in the Tyrrhenian Sea. In the Provencal Basin high POC fluxes linked to the deep convection, with values ranging from -15 to $-30\,\mathrm{g\,C\,m^{-2}\,y^{-1}}$ are modeled. All over the Eastern Basin, F_{POC} is low (around $-1.9\,\mathrm{g\,C\,m^{-2}\,y^{-1}}$), except in the Adriatic Sea where the mean F_{POC} equals $-4.7\,\mathrm{g\,C\,m^{-2}\,y^{-1}}$.

Seasonal variability

The seasonal variability and the spatial distribution of F_{DOC} and F_{POC} differ significantly (Figs. 16 and 18).

Significative DOC fluxes generally occur in winter (Fig. 16). Maximum values of F_{DOC} are reached in early winter in the Provencal sub-Basin and along the continental slopes from autumn to early spring. In several areas (Tyrrhenian and Adriatic Seas, Levantine and Ionian Basins), high downward F_{DOC} values are observed in winter while they are almost null during the rest of the year.

DOC export takes place when DOC rich surface waters plunge or are mixed with poorer deeper waters. Bacteria are the first consumers of DOC, their internal status shapes DOC patterns at Basin scale and DOC accumulation is due to an availability beyond bacterial carbon needs. When the relative C quota of bacteria is the lowest (i.e. lower than N and P quotas), bacteria growth and sustainability are limited by the amount of DOC in their local environment, meaning that bacterial needs in DOC are higher than the available DOC in water. Therefore intracellular quotas of bacteria can help in the identification of regions of potential DOC accumulation.

Figure 17 aims to resume the connection between bacteria and DOC at 100 m depth. In most regions bacteria are depleted in carbon and any input of DOC would lead to an increase bacterial activity and a consumption of this pool. On the opposite in some regions bacteria are rarely limited by carbon, particularly along continenal slopes in the Eastern Basin and in the south Ionian Sea (south of 34° N). In these areas, DOC may not be consumed even at 100 m depth and export may then occurs during the whole year.

High absolute values of F_{POC} at 100 m are calculated from winter to spring in the Alboran Sea and the Provencal sub-Basin (Fig. 18). In the regions associated with the highest downward F_{POC} values (West of 7° E, see Fig. 15, bottom), the maximum occurs in winter (February–March) in the Alboran Sea, and in spring (March–April) in the Algerian Sea and the Provencal sub-Basin. Elsewhere, the maxima are in spring in the Tyrrhenian Sea, the Levantine Basins (except for the Rhodes Gyre where the maximum is earlier in winter) and in the Adriatic Sea.

POC export in the Eastern Basin (excluding the Adriatic Sea) is very weak (even in the Rhodes Gyre) given the fact that POC concentrations stay very low (see Sect. 3.2.2). Our results may however underestimate the actual POC flux in the Eastern bassin as seen when comparing with observation made with sediment traps (see Sect. 4.2).

Export below 200 m

Below 100 m, organic carbon is progressively consumed via the bacterial activity and respiration. At 200 m, the calculated mean export fluxes of total organic carbon are reduced by almost 87 and 64 % compared to those at 100 m, respectively in the Western and Eastern Basins. However, the ratio between export at these two depths is highly variable, depending on the region and the form of organic carbon (see Fig. 19).

For POC (Fig. 19a), the 200 to 100 m ratio is lower than 0.25 (i.e. only 25 % of the carbon exported at 100 m goes below 200 m) in a region including the Alboran Sea, the West Algerian Sea and the Balearic Sea where POC export at 100 m is high (see

Fig. 15, bottom). This ratio is slighly higher but still below 0.3 for the central Algerian Sea and the Adriatic Sea, the Provencal sub-Basin is the only region of high export below 200 m with a ratio about 0.4. In the Tyrrhenian Sea, the Ionian and Levantine Basins, ratio ranges between 0.4 and 0.8 but are associated with low downward POC fluxes below 100 m.

For DOC (Fig. 19b), the ratio is more spatially variable, and in some regions the ratio is higher than 0.4: the Provencal sub-Basin, continental slopes in the Levantine Basin, the North Ionian Basin, the Rhodes Gyre and the Adriatic Sea. Some patches of high ratios are also visible close to the Algerian Coast. Elsewhere the ratio ranges from almost zero (Tyrrhenian Sea, the Alboran Sea) to 0.2 in the Eastern Basin.

4 Discussion

4.1 Model accuracy

Due to the high complexity of the biogeochemical model and the scarcity of data, the assessment of the model's representativeness at the scale of the Mediterranean Sea is a complex task.

This work, however, aims at performing comparisons on several modeled variables, at different time and space scales when in situ measurements were available. If the model and observations are mostly in agreement, some discrepancies have been identified that will now be discussed. In the Adriatic Sea and along the Algerian coast, observed chlorophyll concentrations and primary production patterns are not well reproduced, which may be partly due to the hydrodynamic simulation that do not identify the actual physical structures well. In the most oligotrophic regions, (Levantine, Ionian and Tyrrhenian Seas), modeled chlorophyll does not match the seasonal pattern identified with satellite data, since the higher concentrations modeled are in summer instead of spring. This shortcoming can be largely relativized by the fact that the mean surface chlorophyll in summer equals $0.06 \, \mu g \, L^{-1}$ and does not differ significantly from the

satellite measurement ($0.04\,\mu g\,L^{-1}$). Furthermore, surface chlorophyll in the model is estimated as the mean over the first 10 m of the water column, and therefore includes part of the chlorophyll gradient towards the DCM. Finally, the summer functioning of the surface layer is well reproduced by the model: small phytoplankton are largely dominant and maintain their activity thanks to the microbial loop. Conversely, in regions associated with high nutrient inputs (Ligurian Sea, Alboran Sea) the temporal evolution of surface chlorophyll is reproduced but concentrations are overestimated during the bloom (Fig. 7b and f).

Nutrient concentrations are slightly lower in the model than in observations in almost every vertical layer. This can be attributed to an underestimation of initial nutrient stocks at depth. The model tends to overestimate surface nitrate concentrations during periods of intense stratification (see Sect. 3.1.1). This may be related to an overestimation of nitrification processes, and/or an underestimation of detrital organic matter sinking. Nitrification is, indeed, a linear function with a fixed parameter and does not take into account potential dependancies of the process (e.g. Paulmier et al., 2009). Looking at the vertical attenuation of POC fluxes, it is common to use a power law expressed as $F(z) = F(z = z_0) \times (\frac{z}{z_0})^{-b}$, where $F(z)$ is the depth-dependent POC flux and b a positive coefficient whose values may vary according to the location or the period. In regions of significant export, b values inferred from the model outputs fluctuate between 0.9 in the Provencal sub-Basin and 2.3 for the Algerian Basin. Values of b derived from observations tend to be lower: 0.92 and 1.0 for the Western and Eastern moorings, respectively (Gogou et al., 2014), or 0.75 in the Alboran Sea (Zúñiga et al., 2007). This suggests that the attenuation of POC export flux is too great in the model. Two explanations can be put forward for this: (i) first, the model does not differentiate between small and large detrital particles, and the mean sinking velocity used for simulation may be underestimated, and (ii) second, the model may overestimate particulate organic matter (POM) hydrolysis. As a consequence, the nitrate stock remains too great in the surface water. Finally, the contribution of large phytoplankton (which fuels the POM compartment) to primary production may be underestimated, as suggested by the comparison with Dy-

FaMed data (see Sect. 3.1.2) and with findings from the BOUM cruise in the Eastern Basin (Crombet et al., 2011) and this could be due to an underestimation of phosphate stocks, and/or an overestimation of light attenuation. Thus, though perfectible, this work does provide unique insight into the spatial and temporal variabilities of organic carbon export in the Mediterranean Sea. Seasonal maps of DOC and POC exports at Basin scale are inexistent in both modeling and observational studies. Due to the large uncertainties associated with methodologies dedicated to estimating carbon export from in situ observations, the evaluation of export maps from in situ data is challenging. For particulate organic carbon, trap efficiency is, indeed, regularly questioned in the literature (e.g. Ducklow et al., 2001), whereas the different methods used to estimate DOC export are indirect methods based on strong hypotheses.

4.2 Predominance of dissolved fraction in the organic carbon export

Model results show a preponderance of DOC in the total organic export below both 100 and 200 m depths in most regions of the Mediterranean Sea. This is consistent with the comparisons between POC and DOC exports performed by Santinelli et al. (2013); Copin-Montégut and Avril (1993) or Lefèvre et al. (1996) who estimated that DOC was the main source of remineralization processes in the aphotic layer. One of the main results of this study is that DOC export exceeds POC export in the whole Mediterranean Basin, with the exception of in the Alboran Sea (west of $3°$ W). In the Western Basin, the ratio of DOC over POC export fluxes is comprised between 2 and 5, and is approximately equal to 4 at DyFaMed grid point, where DOC (POC) export at 100 m is 23.5 (5.6) $g\,C\,m^{-2}\,y^{-1}$. Observations at DyFaMed station led to a DOC export estimation of 11.9 $g\,C\,m^{-2}\,y^{-1}$ (Avril, 2002), markedly higher than POC export estimations at 200 m which ranged from 1.2 to 7 $g\,C\,m^{-2}\,y^{-1}$ (Miquel et al., 2011; Copin-Montégut and Avril, 1993). In the Northwestern Basin, the modeled ratio is about 2 at 100 and 200 m, while in the same area a modeling study (Herrmann et al., 2014) led to a ratio at 200 m which ranged from 0.9 to 1.8, even though the corresponding export fluxes were higher than in the present study.

Printer-friendly Version

Interactive Discussion

The ratio between modeled DOC and POC exports at 100 m ranges from 2 to 8 in the Adriatic Sea, with a median value of 5.2. In the same region, a DOC flux of $15.4\,\mathrm{g\,C\,m^{-2}\,y^{-1}}$ was estimated from observations by Santinelli et al. (2013). This is nearly 5 times higher than the measured POC export flux of $3.3\,\mathrm{g\,C\,m^{-2}\,y^{-1}}$, which was, however, sampled during a different period (Boldrin et al., 2002).

In the Eastern Basin, DOC export is regularlty more than 10 times that of POC, due to the very weak POC export and to the high DOC export along the coast and in the open sea. Few observations and estimations are available for this region. In the Northern Ionian Sea, Boldrin et al. (2002) reported low annual POC fluxes at 150 m $(2.4\,\mathrm{g\,C\,m^{-2}\,y^{-1}})$, which are slightly higher than the simulated annual POC fluxes in the same area (1.2 and $0.6\,\mathrm{g\,C\,m^{-2}\,y^{-1}}$ at 100 and 200 m, respectively). In situ measurements of daily POC export across the Mediterranean Sea at 200 m showed strong differences, with lower POC export in the Eastern Basin than in the Western Basin (Moutin and Raimbault, 2002). When compared with the few available measurements of DOC export from the DyFaMed station, the Adriatic Sea, and the Tyrrhenian Sea, the model always provides higher DOC export values. These differences in DOC export may be partly attributable to model failures, but, as already mentioned, high uncertainties are also associated with in situ estimations. For example, DOC export computations from stock differences below the euphotic layer probably underestimate the real flux (Santinelli et al., 2013). If we assume, however, that the different in situ evaluations are consistent with each other, it appears that the highest DOC export occurs in the Adriatic Sea, followed by DyFaMed station (Ligurian Sea) and then by the Tyrhhenian Sea, and the same order can be inferred from the model outputs.

The consistency demonstrated between in situ data of organic carbon export fluxes and the corresponding fluxes provided by the present model has several implications. First, it strengthens the reliability of our results and, in particular, highlights the major role of the dissolved fraction of total organic carbon export below the euphotic layer. In the context of climate change, this has a more far-reaching implication, since the enhanced stratification that should accompany an increase in temperature is expected

to result in an increase of DOC production (Santinelli et al., 2013; Lazzari et al., 2013), and thereby further increase the importance of DOC in the biological carbon pump.

4.3 Relationships between POC and DOC export

Export of POC and DOC fluxes are associated with different processes occurring at different times of the year. As a result, over the whole Mediterranean Sea, 88 % of DOC export occurs between November and February, which is coherent with observations at DyFaMed station where 90 % of annual DOC export was linked to winter mixing (Avril, 2002). By contrast, POC export is more even throughout the year, and during the same period only 23 % of POC is exported. At DyFaMed station, both observed and modeled seasonal signals are dominated by high POC fluxes connected to blooms of large organisms, with a maximum in February–March for in situ data (Miquel et al., 2011), and in April for the model. Finally, a strong correlation between annual primary production and POC export can be evidenced (spearman's rank correlation coefficient is 0.84), while this is not the case for DOC export (correlation below 0.01). The spatial correlation between POC and DOC fluxes is weak. Regions of high POC (DOC) export (see contours in Fig. 15) generally do not match. For example, the Alboran Sea is characterized by high POC export fluxes as well as by relatively low DOC export fluxes. The only areas associated with both high POC and DOC exports are the Algerian coast, the Adriatic coast, the regions of deep convection and a band east of the Balearic Islands. Each of these regions is associated with considerable productivity and high physical variability (high horizontal velocities and deep convection).

4.4 Spatial and time variability of DOC export in the light of processes

Some differences in the mechanisms of DOC export can be identified between regions. For example, in the center of the Ionian Basin, DOC stock in the first 100 m increases from May to November as DOC production processes (mainly exudation by P-limited phytoplankton during summer) dominates DOC consumption (bacterial activ-

ity is limited by nutrients). Destratification in autumn leads to a net export as well as an increase of DOC consumption through bacterial activity, driven by nutrient supply from deep water. During this period, primary production is weak. In the North Western Mediterranean, which is characterized by deep convection events in winter, two dis-
5 tinct periods can be identified in the process of DOC export. During the first period, DOC stocks that accumulated during summer are progressively exported as soon as the water column is destratified (November–December), following a similar process to that already mentioned for the Ionian Basin: during this period, the total DOC stock decreases. The second period occurs in March, when primary production begins to
10 increase while the mixing layer is still deep. In this case, DOC export is concomitant with its production via DOC exudation by phytoplankton during the bloom. DOC export patterns along the Algerian coast and the continental slopes are different, as they occur all year long with particularly high fluxes between October and May. In these regions, DOC stocks above 100 m remain high throughout the year, which is also diagnosed by
15 the rare occurrence of C-limitation of bacteria at 100 m depth (see Fig. 17). This DOC accumulation is mainly due to lateral advection and exudation by small phytoplankton. In these regions, carbon export fluxes are much higher than elsewhere and are mainly associated with downwelling processes.

5 Conclusions

20 A 14 year simulation combining a high resolution physical model (NEMO-MED12) and a biogeochemical model (Eco3M-MED) has been built to study carbon organic production and fate at the scale of the Mediterranean Sea.

The first part of this work focuses on the model skill assessment through an extensive comparison of different model outputs (i.e. chlorophyll, but also nutrients) with available
25 data at various time and space scales. Corresponding results show, in general, a globally satisfying representation of the biogeochemical functioning of the Mediterranean Sea. In the second part of this work, carbon export fluxes are investigated. Previous

estimations of DOC export in the Mediterranean Sea were restricted to specific regions of the Mediterranean Sea (e.g. the Ligurian, Adriatic, Tyrrhenian Seas). We here propose the first Basin-scale view of annual DOC and POC export fluxes, as well as an analysis of their spatial and seasonal variations.

A major result of this modeling study concerns the crucial role of the dissolved fraction in the total organic carbon export. At the Mediterranean scale, DOC export represents about four fifths of total organic carbon fluxes, thereby attesting to its major role in the carbon cycle and the biological pump in the Mediterranean Sea. Regions of non C-limited bacteria are preferential for DOC export, and this is particularly the case for continental slopes and the south Ionian Sea. Export in the Eastern Basin is markedly high despite its lower productivity compared to the Western Basin. By contrast, POC export is closely associated with regions characterized by high productivity. As a consequence, total carbon export in the Eastern Basin is considerably higher than expected as regards its low primary productivity, and barely lower than that of the Western Basin. Results also show high spatial variability in organic carbon fluxes and a temporal uncoupling between POC and DOC exports. This is attributable to the differences in the processes involved in the production and export of POC and DOC.

Further comparisons with observations are clearly necessary to confirm these results, which emphasizes the need for in situ temporal monitoring to properly quantify organic carbon export. This study also identifies the need to examine the microbial food web in detail in order to further investigate the carbon cycle in the Mediterranean Sea. Impacts of potential limitations of the different planktonal functional type could also be adressed in a future work. A thorough analysis of the biogeochemical functionning of the Mediterranean Sea, in the light of the intracellular quotas should also be conducted in future work. Finally, the implementation of an inorganic carbon compartment in the biogeochemical model would close the carbon budget and help in the full characterization of the biological pump.

References

Alekseenko, E., Raybaud, V., Espinasse, B., Carlotti, F., Queguiner, B., Thouvenin, B., Gareau, P., and Baklouti, M.: Seasonal dynamics and stoichiometry of the planktonic community in the NW Mediterranean Sea: a 3D modeling approach, Ocean Dynam., 64, 179–207, 2014. 6151, 6152, 6153, 6154, 6155

Antoine, D., Morel, A., and André, J.: Algal pigment distribution and primary production in the eastern Mediterranean as derived from coastal zone color scanner observations, J. Geophys. Res., 100, 16193–16209, 1995. 6168

Avril, B.: DOC dynamics in the northwestern Mediterranean Sea (DYFAMED site), Deep-Sea Res. Pt. II, 49, 2163–2182, 2002. 6150, 6171, 6178, 6180, 6207

Baklouti, M., Diaz, F., Pinazo, C., Faure, V., and Queguiner, B.: Investigation of mechanistic formulations depicting phytoplankton dynamics for models of marine pelagic ecosystems and description of a new model, Prog. Oceanogr., 71, 1–33, 2006a. 6154

Baklouti, M., Faure, V., Pawlowski, L., and Sciandra, A.: Investigation and sensitivity anlysis of a mechanistic phytoplankton model implemented in a new modular tool (Eco3M) dedicated to biogeochemical modelling, Prog. Oceanogr., 71, 34–58, 2006b. 6152

Baklouti, M., Chevalier, C., Bouvy, M., Corbin, D., Pagano, M., Troussellier, M., and Arfi, R.: A study of plankton dynamics under osmotic stress in the Senegal River Estuary, West Africa, using a 3D mechanistic model, Ecol. Model., 222, 2704–2721, 2011. 6154

Béranger, K., Mortier, L., and Crépon, M.: Seasonal variability of water transport through the Straits of Gibraltar, Sicily and Corsica, derived from a high-resolution model of the Mediterranean circulation, Prog. Oceanogr., 66, 341–364, 2005. 6152

Beuvier, J., Sevault, F., Herrmann, M., Kontoyiannis, H., Ludwig, W., Rixen, M., Stanev, E., Béranger, K., and Somot, S.: Modeling the Mediterranean Sea interannual variability during 1961–2000: focus on the Eastern Mediterranean Transient, J. Geophys. Res.-Oceans, 115, C08017, doi:10.1029/2009JC005950, 2010. 6152, 6156

5 Beuvier, J., Béranger, K., Brossier, C., Somot, S., Sevault, F., Drillet, Y., Bourdallé-Badief, R., Ferry, N., and Lyard, F.: Spreading of the Western Mediterranean Deep Water after winter 2005: time scales and deep cyclone transport, J. Geophys. Res., 117, C07022, doi:10.1029/2011JC007679, 2012a. 6152

Beuvier, J., Lebeaupin Brossier, C., Béranger, K., Arsouze, T., Bourdallé-Badie, R., C., D.,
10 Drillet, Y., Drobinski, P., Lyard, F., Ferry, N., Sevault, F., and Somot, S.: Oceanic component for the modeling of the regional Mediterranean Eart System, Mercator Ocean Quarterly Newsletter, 46, 60–66, 2012b. 6151, 6152, 6156

Boldrin, A., Miserocchi, S., Rabitti, S., Turchetto, M., Balboni, V., and Socal, G.: Particulate matter in the southern Adriatic and Ionian Sea: characterisation and downward fluxes, J.
15 Marine Syst., 33, 389–410, 2002. 6179

Bopp, L., Monfray, P., Aumont, O., Dufresne, J., Le Treut, H., Madec, G., Terray, L., and Orr, J.: Potential climate change on marine export production, Global Biogeochem. Cy., 15, 81–99, 2001. 6151

Bosc, E., Bricaud, A., and Antoine, D.: Seasonal and interannual variability in algal biomass
20 and primary production in the Mediterranean Sea, as derived from 4 years of SeaWiFS observations, Global Biogeochem. Cy., 18, GB1005, doi:10.1029/2003GB002034, 2004. 6157, 6168, 6194

Buesseler, K.: Do upper-ocean sediment traps provide an accurate record of particle flux?, Nature, 353, 420–423, 1991. 6150

25 Carlson, C., Ducklow, H., and Michaels, A.: Annual flux of dissolved organic carbon from the euphotic zone in the northwestern Sargasso Sea, Nature, 371, 405–408, 1994. 6150

Claustre, H., Morel, A., Hooker, S., Babin, M., Antoine, D., Oubelkheir, K., Bricaud, A., Leblanc, K., Queguiner, B., and Maritorena, S.: Is desert dust making oligotrophic waters greener?, Geophys. Res. Lett., 29, 107-1–107-4, 2002. 6157

30 Copin-Montégut, G. and Avril, B.: Vertical distribution and temporal variation of dissolved organic carbon in the North-Western Mediterranean Sea, Deep-Sea Res. Pt. I, 40, 1963–1972, 1993. 6150, 6178

New insights into the organic carbon export in the Mediterranean Sea from 3-D modeling

A. Guyennon et al.

Title Page

Abstract	Introduction
Conclusions	References
Tables	Figures

◄◄　　►►

◄　　►

Back　Close

Full Screen / Esc

Printer-friendly Version

Interactive Discussion

Crise, A., Crispi, G., and Mauri, E.: A seasonal three-dimensional study of the nitrogen cycle in the Mediterranean Sea: Part I. Model implementation and numerical results, J. Marine Syst., 18, 287–312, 1998. 6151

Crispi, G., Crise, A., and Solidoro, C.: Three-dimensional oligotrophic ecosystem models driven by physical forcing: the Mediterranean Sea case, Environ. Modell. Softw., 13, 483–490, 1998. 6151

Crombet, Y., Leblanc, K., Quéguiner, B., Moutin, T., Rimmelin, P., Ras, J., Claustre, H., Leblond, N., Oriol, L., and Pujo-Pay, M.: Deep silicon maxima in the stratified oligotrophic Mediterranean Sea, Biogeosciences, 8, 459–475, doi:10.5194/bg-8-459-2011, 2011. 6178

D'Ortenzio, F. and Ribera d'Alcalà, M.: On the trophic regimes of the Mediterranean Sea: a satellite analysis, Biogeosciences, 6, 139–148, doi:10.5194/bg-6-139-2009, 2009. 6166

D'Ortenzio, F., Marullo, S., Ragni, M., Ribera d'Alcalà, M., and Santoleri, R.: Validation of empirical SeaWiFS algorithms for chlorophyll *a* retrieval in the Mediterranean Sea: a case study for oligotrophic seas, Remote Sens. Environ., 82, 79–94, 2002. 6157

Droop, M.: Vitamin B12 and marine ecology, IV. The kinetics of uptake, growth and inhibition in Monochrysis lutheri, J. Mar. Biol. Assoc. UK, 48, 689–733, 1968. 6154

Ducklow, H., Steinberg, D., and Buesseler, K.: Upper ocean carbon export and the biological pump, Oceanography-Washington DC-Oceanography Society, 14, 50–58, 2001. 6178

Eppley, R. and Peterson, B.: Particulate organic matter flux and planktonic new production in the deep ocean, Nature, 282, 677–680, 1979. 6150

Fasham, M., Flynn, K., Pondaven, P., Anderson, T., and Boyd, P.: Development of a robust marine ecosystem model to predict the role of iron in biogeochemical cycles: a comparison of results for iron-replete and iron-limited areas, and the SOIREE iron-enrichment experiment, Deep-Sea Res. Pt. I, 53, 333–366, 2006. 6155

Garcia, H. E., Locarnini, R., Boyer, T., and Antonov, J.: World Ocean Atlas 2005, Vol. 4, Nutrients (Phosphate, Nitrate, Silicate), 2006. 6155

Geider, R., MacIntyre, H., and Kana, T.: A dynamic regulatory model of phytoplankton acclimation to light, nutrients, and temperature, Limnol. Oceanogr., 43, 679–694, 1998. 6154

Gogou, A., Sanchez-Vidal, A., Durrieu de Madron, X., Stavrakakis, S., Calafat, A. M., Stabholz, M., Psarra, S., Canals, M., Heussner, S., Stavrakaki, I. et al.: Carbon flux to the deep in three open sites of the Southern European Seas (SES), J. Marine Syst., 129, 224–233, 2014. 6177

Title Page

Abstract | Introduction

Conclusions | References

Tables | Figures

◄◄ | ►►

◄ | ►

Back | Close

Full Screen / Esc

Printer-friendly Version

Interactive Discussion

Gómez, F.: The role of the exchanges through the Strait of Gibraltar on the budget of elements in the Western Mediterranean Sea: consequences of human-induced modifications, Mar. Pollut. Bull., 46, 685–694, 2003. 6155

Hansell, D. and Carlson, C.: Marine dissolved organic matter and the carbon cycle, Oceanography, 15, 685–716, 2001. 6150

Hansell, D., Carlson, C., and Suzuki, Y.: Dissolved organic carbon export with North Pacific Intermediate Water formation, Global Biogeochem. Cy., 16, 7-1–7-8, 2002. 6150

Hansell, D., Repeta, D., Carlson, C., and Schlitzer, R.: Dissolved organic matter in the ocean: a controversy stimulates new insights, Oceanography, 22, 202–211, 2009. 6150

Herrmann, M., Somot, S., Sevault, F., Estournel, C., and Déqué, M.: Modeling the deep convection in the northwestern Mediterranean Sea using an eddy-permitting and an eddy-resolving model: case study of winter 1986–1987, J. Geophys. Res.-Oceans, 113, C04011, doi:10.1029/2006JC003991, 2008. 6152

Herrmann, M., Diaz, F., Estournel, C., Marsaleix, P., and Ulses, C.: Impact of atmospheric and oceanic interannual variability on the Northwestern Mediterranean Sea pelagic planktonic ecosystem and associated carbon cycle, J. Geophys. Res.-Oceans, 118, 1–22, 2014. 6178

Holling, C.: Some characteristics of simple types of predation and parsitism, The Cand. Entomol., 91, 385–398, 1959. 6154

Kooijman, S. A. L. M.: Dynamic Energy and Mass Budgets in Biological Systems, Cambridge University Press, Cambridge, UK, 2000. 6154

Lavigne, H., D'Ortenzio, F., Migon, C., Claustre, H., Testor, P., d'Alcalà, M., Lavezza, R., Houpert, L., and Prieur, L.: Enhancing the comprehension of mixed layer depth control on the Mediterranean phytoplankton phenology, J. Geophys. Res.-Oceans, 118, 3416–3430, 2013. 6166

Lazzari, P., Solidoro, C., Ibello, V., Salon, S., Teruzzi, A., Béranger, K., Colella, S., and Crise, A.: Seasonal and inter-annual variability of plankton chlorophyll and primary production in the Mediterranean Sea: a modelling approach, Biogeosciences, 9, 217–233, doi:10.5194/bg-9-217-2012, 2012. 6165, 6168

Lazzari, P., Mattia, G., Solidoro, C., Salon, S., Crise, A., Zavatarelli, M., Oddo, P., and Vichi, M.: The impacts of climate change and environmental management policies on the trophic regimes in the Mediterranean Sea: scenario analyses, J. Marine Syst., 135, 137–149, 2013. 6151, 6180

Le Quéré, C., Takahashi, T., Buitenhuis, E., Rödenbeck, C., and Sutherland, S.: Impact of climate change and variability on the global oceanic sink of CO_2, Global Biogeochem. Cy., 24, 2016–2040, 2010. 6151

Le Quéré, C. L., Harrison, S., P., C., Buitenhuis, E., Aumont, O., Bopp, L., Claustre, H., Cotrim Da Cunha, L., Geider, R., Giraud, X., Klaas, C., Kohfeld, K. E., Legendre, L., Manizza, M., Platt, T., Rivkin, R. B., Sathyendranath, S., Uitz, J., Watson, A. J., and Wolf-Gladrow, D.: Ecosystem dynamics based on plankton functional types for global ocean biogeochemistry models, Glob. Change Biol., 11, 2016–2040, 2005. 6153

Lebeaupin Brossier, C., Béranger, K., Deltel, C., and Drobinski, P.: The Mediterranean response to different space–time resolution atmospheric forcings using perpetual mode sensitivity simulations, Ocean Model., 36, 1–25, 2011. 6152

Leblanc, K., Quéguiner, B., Garcia, N., Rimmelin, P., and Raimbault, P.: Silicon cycle in the NW Mediterranean Sea: seasonal study of a coastal oligotrophic site, Oceanol. Acta, 26, 339–355, 2003. 6153

Lefèvre, D., Denis, M., Lambert, C., and Miquel, J.: Is DOC the main source of organic matter remineraliztion in the ocean water column?, J. Marine Syst., 7, 281–291, 1996. 6178

Ludwig, W.: Continental Erosion and River Transport of Organic Carbon to the World's Oceans, Ph.D. thesis, Université Louis Pasteur de Strasbourg, 1996. 6156

Ludwig, W., Dumont, E., Meybeck, M., and Heussner, S.: River discharges of water and nutrients to the Mediterranean and Black Sea: major drivers for ecosystem changes during past and future decades?, Prog. Oceanogr., 80, 199–217, 2009. 6156

Macías, D., Stips, A., and Garcia-Gorriz, E.: The relevance of deep chlorophyll maximum in the open Mediterranean Sea evaluated through 3D hydrodynamic-biogeochemical coupled simulations, Ecol. Model., 281, 26–37, 2014. 6151

Madec, G. and The-NEMO-Team: NEMO Ocean Engine, Note du pole de modélisation de l'IPSL, 27, 1228–1619, 2008. 6152

Magazzu, G. and Decembrini, F.: Primary production, biomass and abundance of phototrophic picoplankton in the Mediterranean Sea: a review, Aquat. Microb. Ecol., 9, 97–104, 1995. 6169

Maier-Reimer, E., Mikolajewicz, U., and Winguth, A.: Future ocean uptake of CO_2: interaction between ocean circulation and biology, Clim. Dynam., 12, 711–722, 1996. 6151

Marshall, J. and Schott, F.: Open-ocean convection: observations, theory, and models, Rev. Geophys., 37, 1–64, 1999. 6158

New insights into the organic carbon export in the Mediterranean Sea from 3-D modeling

A. Guyennon et al.

Marty, J. and Chiavérini, J.: Seasonal and interannual variations in phytoplankton production at DYFAMED time-series station, northwestern Mediterranean Sea, Deep-Sea Res. Pt. II, 49, 2017–2030, 2002. 6169, 6205

Marty, J. C. and Chiavérini, J.: Hydrological changes in the Ligurian Sea (NW Mediterranean, DYFAMED site) during 1995–2007 and biogeochemical consequences, Biogeosciences, 7, 2117–2128, doi:10.5194/bg-7-2117-2010, 2010. 6167, 6196, 6199, 6200, 6203

Marty, J., Chiavérini, J., Pizay, M., and Avril, B.: Seasonal and interannual dynamics of nutrients and phytoplankton pigments in the western Mediterranean Sea at the DYFAMED time-series station (1991–1999), Deep-Sea Res. Pt. II, 49, 1965–1985, 2002. 6167

Mattia, G., Zavatarelli, M., Vichi, M., and Oddo, P.: The Eastern Mediterranean Sea biogeochemical dynamics in the 1990s: a numerical study, J. Geophys. Res.-Oceans, 118, 2231–2248, 2013. 6151, 6165

Meador, T., Gogou, A., Spyres, G., Herndl, G., Krasakopoulou, E., Psarra, S., Yokokawa, T., De Corte, D., Zervakis, V., and Repeta, D.: Biogeochemical relationships between ultrafiltered dissolved organic matter and picoplankton activity in the Eastern Mediterranean Sea, Deep-Sea Res. Pt. II, 57, 1460–1477, 2010. 6156

Millot, C. and Taupier-Letage, I.: Circulation in the Mediterranean Sea, in: The Mediterranean Sea, Springer, 29–66, 2005. 6196

Miquel, J., Martín, J., Gasser, B., Rodriguez-y Baena, A., Toubal, T., and Fowler, S.: Dynamics of particle flux and carbon export in the northwestern Mediterranean Sea: a two decade time-series study at the DYFAMED site, Prog. Oceanogr., 91, 461–481, 2011. 6178, 6180

Morel, A.: Optical modeling of the upper ocean in relation to its biogenous matter content (case I waters), J. Geophys. Res.-Oceans, 93, 10749–10768, 1988. 6155

Moutin, T. and Prieur, L.: Influence of anticyclonic eddies on the Biogeochemistry from the Oligotrophic to the Ultraoligotrophic Mediterranean (BOUM cruise), Biogeosciences, 9, 3827–3855, doi:10.5194/bg-9-3827-2012, 2012. 6160, 6197, 6198

Moutin, T. and Raimbault, P.: Primary production, carbon export and nutrients availability in Western and Eastern Mediterranean Sea in early summer 1996 (MINOS cruise), J. Marine Syst., 33, 273–288, 2002. 6150, 6168, 6179

Moutin, T., Van Wambeke, F., and Prieur, L.: Introduction to the Biogeochemistry from the Oligotrophic to the Ultraoligotrophic Mediterranean (BOUM) experiment, Biogeosciences, 9, 3817–3825, doi:10.5194/bg-9-3817-2012, 2012. 6158, 6196, 6197, 6198

Palmiéri, J.: Modélisation Biogéochimique de la Mer Méditerranée avec le Modèle Régional Couplé NEMO-MED12/PISCES, Ph.D. thesis, Université de Versailles Saint-Quentin, France, 2014. 6156

Palmiéri, J., Orr, J. C., Dutay, J.-C., Béranger, K., Schneider, A., Beuvier, J., and Somot, S.: Simulated anthropogenic CO_2 storage and acidification of the Mediterranean Sea, Biogeosciences, 12, 781–802, doi:10.5194/bg-12-781-2015, 2015a. 6152

Palmiéri, J., Le Vu, B., Dutay, J., Bopp, L., Béranger, K., Beuvier, J., Somot, S., and Éthé, C.: Biogeochemical modelling of the Mediterranean Sea with PISCES MED-12 model, GMD, in preparation, 2015b. 6156

Paulmier, A., Kriest, I., and Oschlies, A.: Stoichiometries of remineralisation and denitrification in global biogeochemical ocean models, Biogeosciences, 6, 923–935, doi:10.5194/bg-6-923-2009, 2009. 6177

Prowe, A., Pahlow, M., Dutkiewicz, S., Follows, M., and Oschlies, A.: Top-down control of marine phytoplankton diversity in a global ecosystem model, Prog. Oceanogr., 101, 1–13, 2012. 6154

Pujo-Pay, M., Conan, P., Oriol, L., Cornet-Barthaux, V., Falco, C., Ghiglione, J.-F., Goyet, C., Moutin, T., and Prieur, L.: Integrated survey of elemental stoichiometry (C, N, P) from the western to eastern Mediterranean Sea, Biogeosciences, 8, 883–899, doi:10.5194/bg-8-883-2011, 2011. 6160

Santinelli, C., Hansell, D. A., and Ribera d'Alcala, M., R.: Influence of stratification on marine dissolved organic carbon (DOC) dynamics: the Mediterranean Sea case, Prog. Oceanogr., 119, 68–77, 2013. 6150, 6178, 6179, 6180

Sarmiento, J. and Gruber, N.: Ocean Biogeochemical Dynamics, vol. 1015, Princeton University Press Princeton, 2006. 6150, 6151

Sarmiento, J., Hughes, T., Stouffer, R., and Manabe, S.: Simulated response of the ocean carbon cycle to anthropogenic climate warming, Nature, 393, 245–249, 1998. 6151

Schaap, D. and Lowry, R.: SeaDataNet–Pan-European infrastructure for marine and ocean data management: unified access to distributed data sets, International Journal of Digital Earth, 3, 50–69, 2010. 6155

Siegenthaler, U. and Sarmiento, J.: Atmospheric carbon dioxide and the ocean, Nature, 365, 119–125, 1993. 6149

New insights into the organic carbon export in the Mediterranean Sea from 3-D modeling

A. Guyennon et al.

Title Page

Abstract	Introduction
Conclusions	References
Tables	Figures

◄◄   ►►

◄   ►

Back   Close

Full Screen / Esc

Printer-friendly Version

Interactive Discussion

Siokou-Frangou, I., Christaki, U., Mazzocchi, M. G., Montresor, M., Ribera d'Alcalá, M., Vaqué, D., and Zingone, A.: Plankton in the open Mediterranean Sea: a review, Biogeosciences, 7, 1543–1586, doi:10.5194/bg-7-1543-2010, 2010. 6153, 6169

Somot, S., Sevault, F., and Déqué, M.: Transient climate change scenario simulation of the Mediterranean Sea for the twenty-first century using a high-resolution ocean circulation model, Clim. Dynam., 27, 851–879, 2006. 6152

Soto-Navarro, J., Somot, S., Sevault, F., Beuvier, J., Criado-Aldeanueva, F., García-Lafuente, J., and Béranger, K.: Evaluation of regional ocean circulation models for the Mediterranean Sea at the Strait of Gibraltar: volume transport and thermohaline properties of the outflow, Clim. Dynam., 44, 1–16, 2014. 6152

Sournia, A.: La production primaire planctonique en Méditerranée; essai de mise à jour, Cooperative Investigations in the Mediterranean, International Coordinator and Operational Unit; Étude en commun de la Méditerranée, Coordonnateur international et Unité opérationnelle, 1973. 6168

Thingstad, T., Hagström, A., and Rassoulzadegan, F.: Accumulation of degradable DOC in surface waters: is it caused by a malfunctioning microbial loop?, Limnol. Oceanogr., 42, 398–404, 1997. 6150

Thingstad, T., Krom, M., Mantoura, R., Flaten, G., Groom, S., Herut, B., Kress, N., Law, C., Pasternak, A., Pitta, P., Psarra, S., Rassoulzadegan, F., Tanaka, T., Tselepides, A., Wassmann, P., Woodward, E. M. S., Wexels Riser, C., Zodiatis, G., and Zohary, T.: Nature of phosphorus limitation in the ultraoligotrophic Eastern Mediterranean, Science, 309, 1068–1071, 2005. 6150

Toggweiler, J., Gnanadesikan, A., Carson, S., Murnane, R., and Sarmiento, J.: Representation of the carbon cycle in box models and GCMs: 1. Solubility pump, Global Biogeochem. Cy., 17, 26-1–26-11, 2003. 6151

Tugrul, S. and Besiktepe, S.: Nutrient Exchange Fluxes Between the Black Sea and the Mediterranean Through the Turkish Strait System (Marmara Sea, Bosphorus and Dardanelles), CIESM, 2007. 6156

Uitz, J., Stramski, D., Gentili, B., D'Ortenzio, F., and Claustre, H.: Estimates of phytoplankton class-specific and total primary production in the Mediterranean Sea from satellite ocean color observations, Global Biogeochem. Cy., 26, GB2024, doi:10.1029/2011GB004055, 2012. 6168, 6194

Vallina, S., Ward, B., Dutkiewicz, S., and Follows, M.: Maximal feeding with active prey-switching: a kill-the-winner functional response and its effect on global diversity and biogeography, Prog. Oceanogr., 120, 93–109, 2014. 6154

Van Wambeke, F., Christaki, U., Giannakourou, A., Moutin, T., and Souvemerzoglou, K.: Longitudinal and vertical trends of bacterial limitation by phosphorus and carbon in the Mediterranean Sea, Microb. Ecol., 43, 119–133, 2002. 6150

Vichi, M., Pinardi, N., and Masina, S.: A generalized model of pelagic biogeochemistry for the global ocean ecosystem, Part I: theory, J. Marine Syst., 64, 89–109, 2007. 6155

Volpe, G., Santoleri, R., Vellucci, V., Ribera d'Alcala, M., Marullo, S., and d'Ortenzio, F.: The colour of the Mediterranean Sea: Global versus regional bio-optical algorithms evaluation and implication for satellite chlorophyll estimates, Remote Sens. Environ., 107, 625–638, 2007. 6157

Vörösmarty, C. J.,Fekete, B. M., and Tucker, B. A.: Global River Discharge Database, RivDis, Tech. Rep., 1996. 6156

Zúñiga, D., Calafat, A., Sanchez-Vidal, A., Canals, M., Price, B., Heussner, S., and Miserocchi, S.: Particulate organic carbon budget in the open Algero-Balearic Basin (Western Mediterranean): assessment from a one-year sediment trap experiment, Deep-Sea Res. Pt. I, 54, 1530–1548, 2007. 6177

Table 1. Mean nutrients concentrations observed and calculated in the Western and Eastern Basins from BOUM cruise. Value in brackets is the SD, BQL stands for Below the Quantification Limit ($0.05\,\mu mol\,L^{-1}$).

		Model		Observations	
		West	East	West	East
0–30 m	NO_3	0.4 [0.2]	0.6 [0.1]	BQL	BQL
	PO_4	0.002 [0]	0.002 [0]	BQL	BQL
250–1500 m	NO_3	6.3 [1]	4.7 [0.4]	8.7 [1.1]	5.3 [1.4]
	PO_4	0.27 [0.1]	0.14 [0]	0.37 [0.1]	0.18 [0.1]
> 1500 m	NO_3	7.7 [0.1]	5.4 [0.2]	8.9 [0.5]	5.0 [0.5]
	PO_4	0.34 [0]	0.15 [0]	0.38 [0]	0.16 [0]
Range	NO_3	[0; 7.8]	[0.36; 5.7]	[BQL; 9.8]	[BQL; 6.3]
	PO_4	[0; 0.34]	[0; 0.18]	[BQL; 0.44]	[BQL; 0.28]

Table 2. Mean nutrients concentrations at the DyFaMed site for different layers from observations and model. Values in brackets give the range of observed or calculated concentrations during the period of comparison. The spatial RMSD is calculated for the 8 neighboor points with mean concentrations and in brackets is the maximum RMSD during the period of comparison.

	NO_3			PO_4		
	Spatial RMSD	Model (mNO_3)	Observations (oNO_3)	Spatial RMSD	Model (mPO_4)	Observations (oPO_4)
0–30 m	0.03 [0.42]	1.2 [0.04–4.2]	1.0 [BQL–6.5]	0.003 [0.01]	0.008 [0–0.07]	0.05 [BQL–0.26]
30–100 m	0.10 [0.49]	3.0 [0.09–6.1]	3.8 [BQL–8]	0.003 [0.02]	0.02 [0–0.18]	0.14 [BQL–0.37]
100–250 m	0.13 [0.49]	5.3 [1.7–6.6]	6.6 [1.6–9.6]	0.01 [0.04]	0.16 [0–0.32]	0.28 [BQL–0.42]
250–500 m	0.03 [0.19]	6.4 [5.0–7.1]	7.9 [5.1–9.7]	0.003 [0.2]	0.31 [0.16–0.33]	0.35 [0.2–0.46]
> 1000 m	0.004 [0.008]	7.8 [7.4–7.9]	7.6 [5.4–9.4]	2×10^{-4} [3×10^{-4}]	0.34 [0.33–0.34]	0.36 [0.24–0.46]

Full Screen / Esc

Printer-friendly Version

Interactive Discussion

Table 3. Integrated gross primary production (mIPP in $g\,C\,m^{-2}\,y^{-1}$) for different regions of the Mediterranean Sea calculated by the model and taken from Bosc et al. (2004) and Uitz et al. (2012).

Region	Model	Uitz et al. (2012) v1	Bosc et al. (2004)
Alboran Sea	222	150	230
Gulf of Lion	182	97	194
Balearic Sea	145	80	167
Algero-Provencal Basin	123	78	153
Ligurian Sea	109	80	165
Algerian Basin	107	78	163
Adriatic Sea	102	71	182
Tyrrhenian Sea	66	67	137
South Levantine Basin	65	59	105
North Levantine Basin	63	60	106
South Ionian Sea	60	61	115
North Ionian Sea	55	63	126
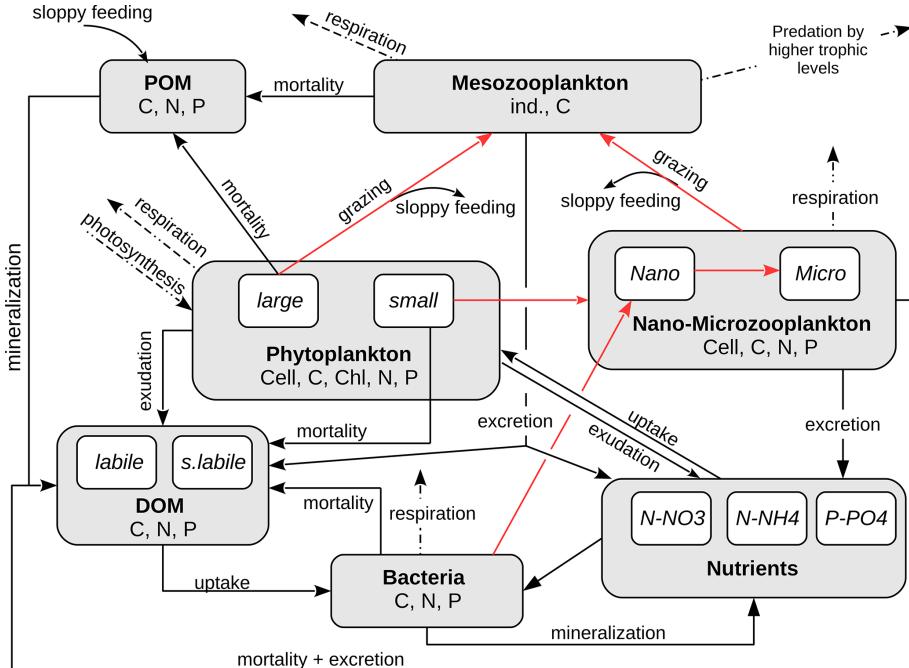
Figure 1. Conceptual diagram of the biogeochemical model Eco3M-MED. Grey boxes represent major compartments and white boxes sub-compartments. State variables for each sub-compartment are listed at the bottom of compartment boxes. Red arrows indicate grazing processes from the prey to the predator.
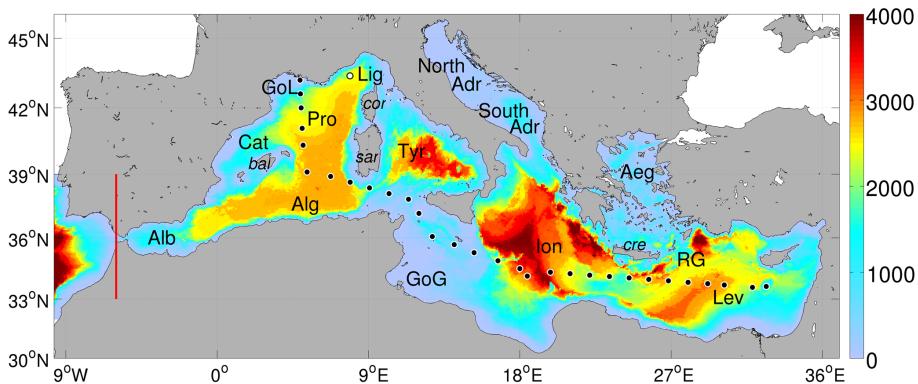
Figure 2. Bathymetry of the grid in meters, black dots represent the BOUM cruise stations (Moutin et al., 2012) while white dot is DyFaMed position (Marty and Chiavérini, 2010). The area West of the red line constitutes the buffer-zone. Acronymes indicates different sub-Basin names and islands (in italic). Terminology is taken from (Millot and Taupier-Letage, 2005). From West to East, **Alb** stands for Alboran Sea, **Cat** the Catalan Sea, **GoL** for the Gulf of Lions, **Pro** the Provencal sub-Basin, **Alg** the Algerian Basin, **Lig** for the Ligurian Sea, **Tyr** for the Tyrrhenian Sea, **GoG** for the Gulf of Gabes, **North Adr** and **South Adr** for the North and South Adriatic Sea respectively, **Ion** for the Ionian sub-Basin, **Aeg** for the Aegan Sea, **Lev** the Levantine sub-Basin and **RG** the Rhodes Gyre. Major islands names are also plotted, *bal* stands for the Balearic islands, *sar* for Sardinia, *Cor* for corsica, *cre* for Crete.

Full Screen / Esc
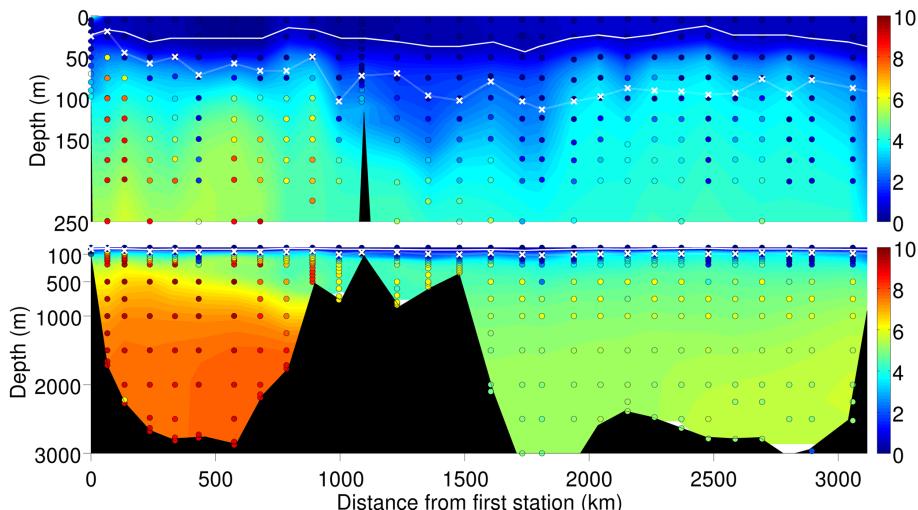
Figure 3. BOUM NO_3 transect (Moutin et al., 2012). The top figure is a detail of the lower figure. Model outputs are in shaded colors; in situ data are colored circles. Model outputs correspond to the daily outputs averaged over the BOUM cruise period. White crosses represent the data-derived depth of the top nitracline as defined in Moutin and Prieur (2012). The white line indicates the top nitracline from model outputs.
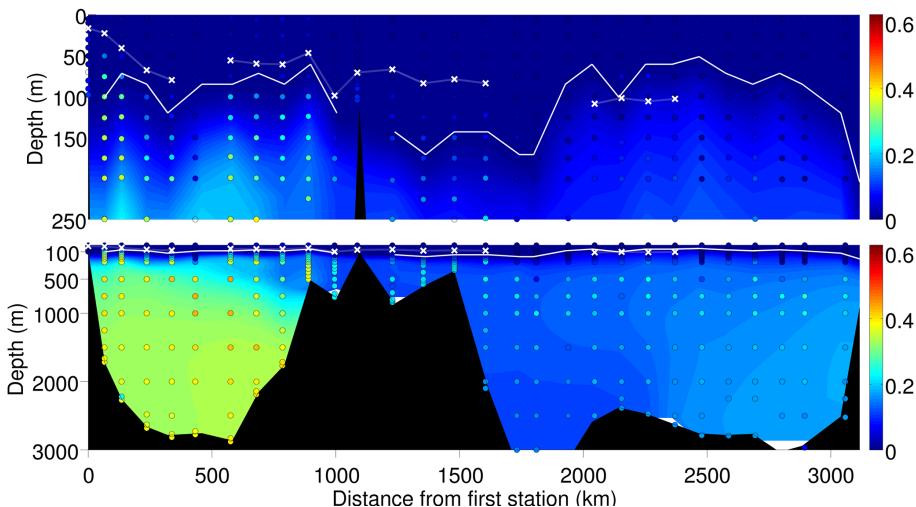
Figure 4. BOUM PO$_4$ transect (Moutin et al., 2012). The top figure is a detail of the lower figure. Model outputs are in shaded colors; in situ data are colored circles. Model outputs correspond to the daily outputs averaged over the BOUM cruise period. The color scale respects the Redfield ratio between nitrate and phosphate. White crosses represent the data-derived depth of the top phosphacline as defined in Moutin and Prieur (2012). The white line is the top phosphacline from model outputs.
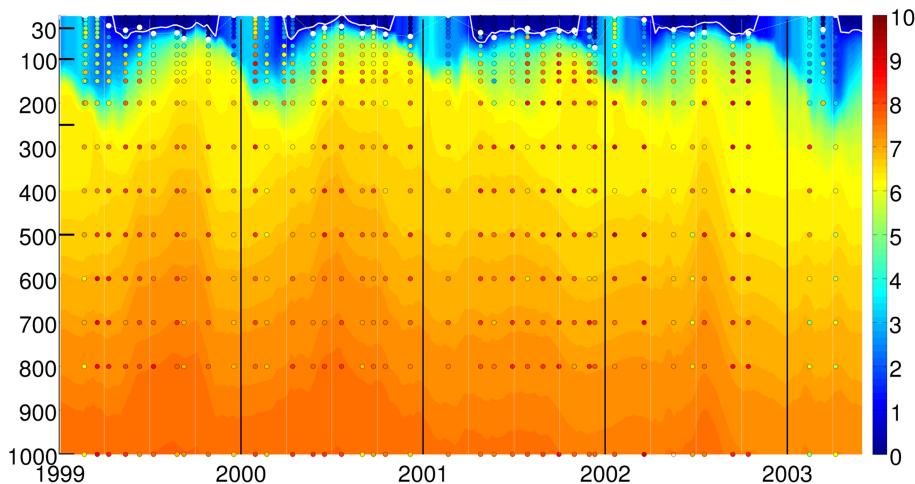
Figure 5. Time evolution of vertical concentrations of nitrate in $\mu mol\,L^{-1}$ at the DyFaMed site. Model outputs are in shaded colors, in situ data in colored dots (Marty and Chiavérini, 2010). $1\,\mu mol\,L^{-1}$ isolines are plotted in white, line is calculated from model outputs, dots from data.
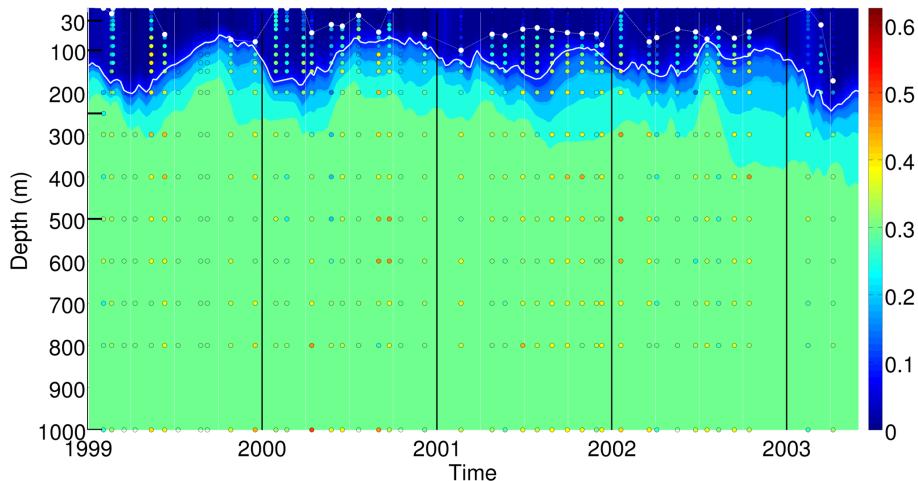
Figure 6. Time evolution of vertical concentrations of phosphate in $\mu mol\,L^{-1}$ at the DyFaMed site. Model outputs are in shaded colors, in situ data in colored dots (Marty and Chiavérini, 2010). $0.1\,\mu mol\,L^{-1}$ isolines are plotted in white, line is calculated from model outputs, dots from data.
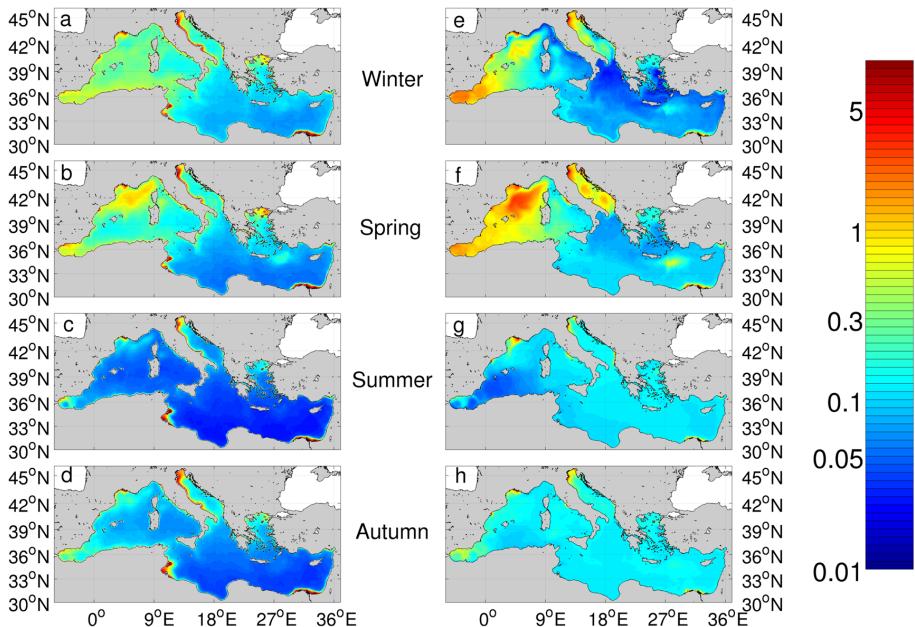
Figure 7. Maps of mean surface chlorophyll concentrations ($\mu g\,L^{-1}$) from satellite (left) and model (right). Means are made over the season given in the central column, model chlorophyll is averaged over the first 10 m of the water column. Period used is 2002–2011 for both model outputs and satellite data.
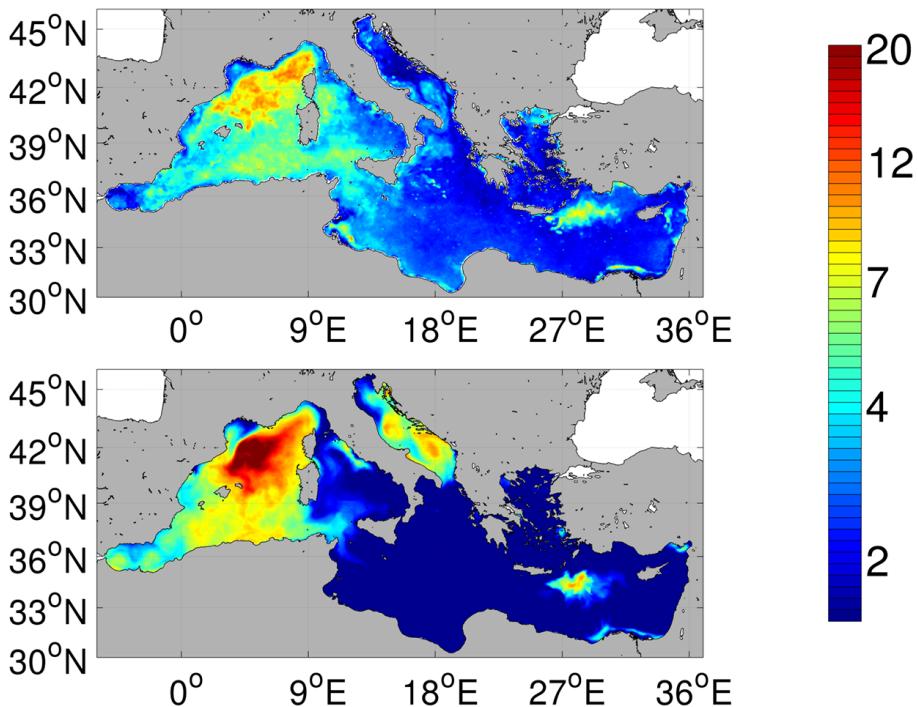
Figure 8. Maps of ratio between annual maximum and annual median for satellite (top) and model (bottom) chlorohyll concentrations over the 2002–2011 period.

Title Page

Abstract | Introduction

Conclusions | References

Tables | Figures

◄ | ►►

◄ | ►

Back | Close

Full Screen / Esc

Printer-friendly Version

Interactive Discussion
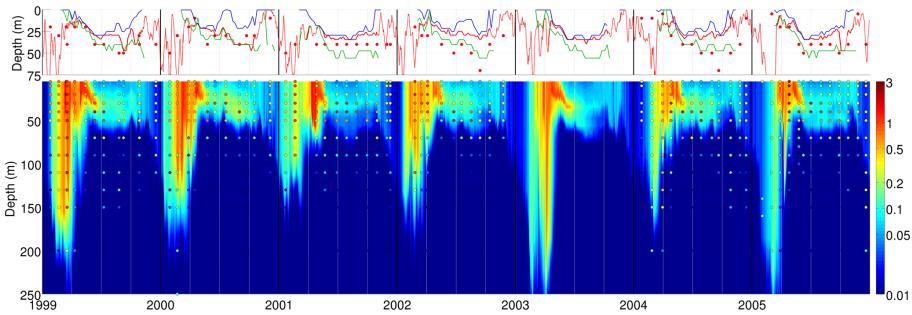
Figure 9. Time evolution of vertical concentrations of chlorophyll ($\mu g\,L^{-1}$) at the DyFaMed site, with model outputs in shaded colors and in situ data in colored dots (Marty and Chiavérini, 2010). On top, the depth of chlorophyll maximum is represented with red dots for in situ data and the red line for the model. When maximum is not obvious (see text), the line is dotted. Depths of maximum chlorophyll for small phytoplankton (blue) and large plankton (green) are also plotted.
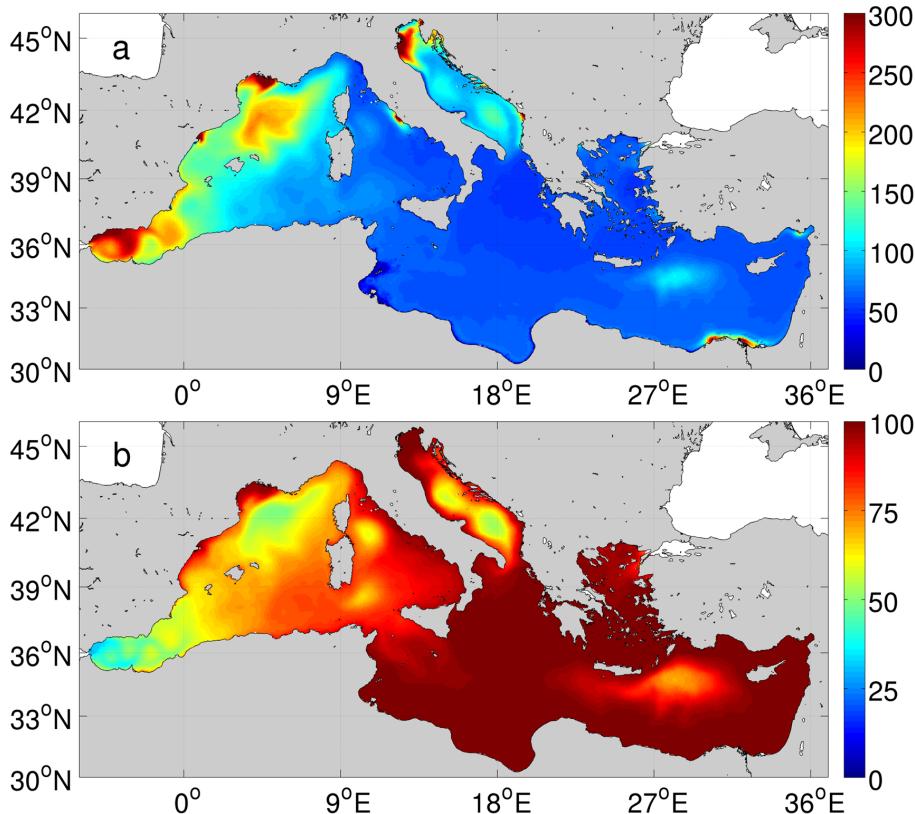
Figure 10. Annual gross primary production calculated over the 2000–2012 period and integrated along the whole water column, in $g\,C\,m^{-2}\,y^{-1}$ **(a)**, proportion of production due to small phytoplankton group, in % **(b)**.

Title Page

Abstract | Introduction

Conclusions | References

Tables | Figures

|◄ | ►|

◄ | ►

Back | Close

Full Screen / Esc

Printer-friendly Version

Interactive Discussion
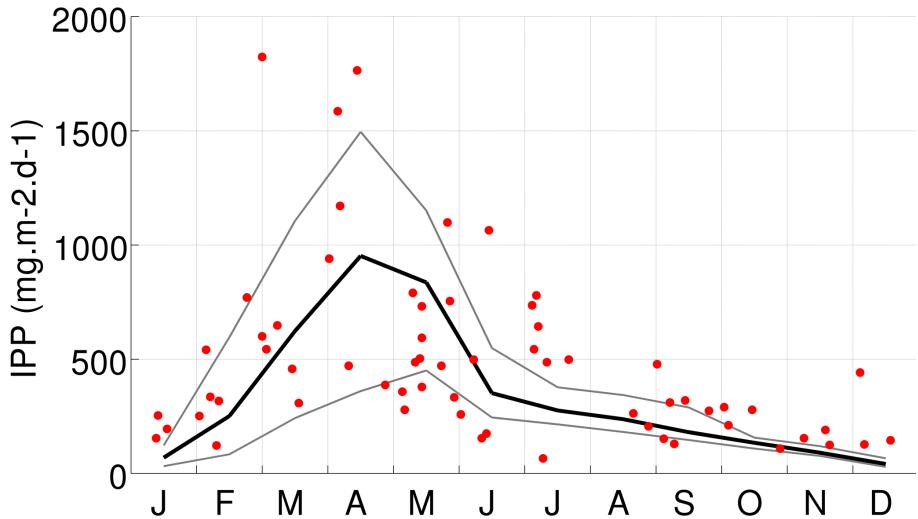
Figure 11. Time evolution of monthly integrated gross primary production in mg C^{-2} d^{-1}. Red dots are values (depth integrated 0–100 m) reproduced from Marty and Chiavérini (2002), the black line is the mean over the 2000–2012 period and grey are lines inter-annual maximum and minimum for every month.
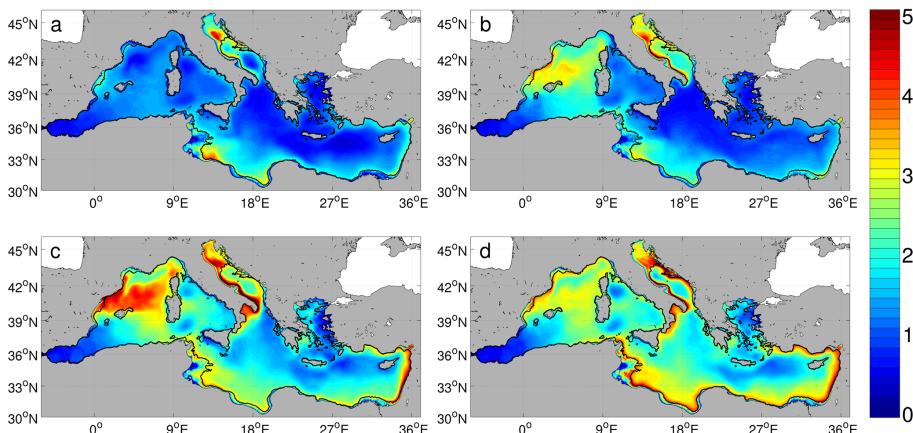
Figure 12. Modeled dissolved organic carbon inventory ($mol\,m^{-2}$) integrated over the first 100 m. Maps are averaged over the 2000–2012 period on every season (**a**: winter, **b**: spring, **c**: summer, **d**: autumn). Black lines are the 100 m isolines.
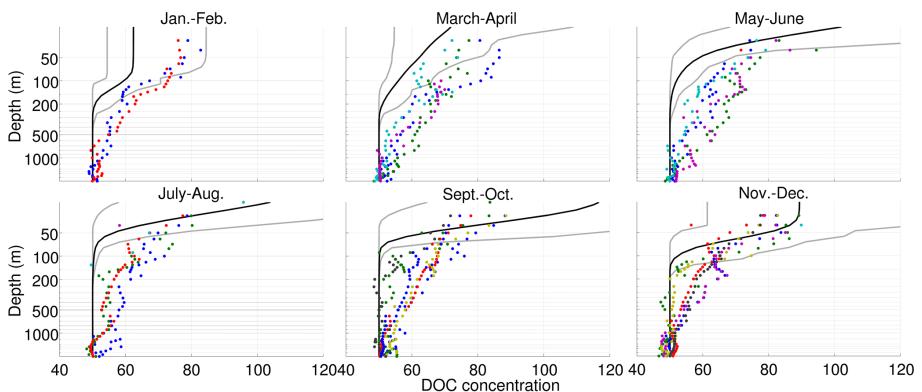
Figure 13. Vertical profiles of total DOC (μmol L^{-1}) at DyFaMed site. For each panel in situ data are plotted as dots, colors account for different time of sampling. Model DOC are weekly averaged outputs. Black line is the mean of model DOC over the period, grey lines are the maximum and minimum concentrations for each depth. In situ data cover the 1991–1993 period (Avril, 2002), model outputs cover 2000–2012.
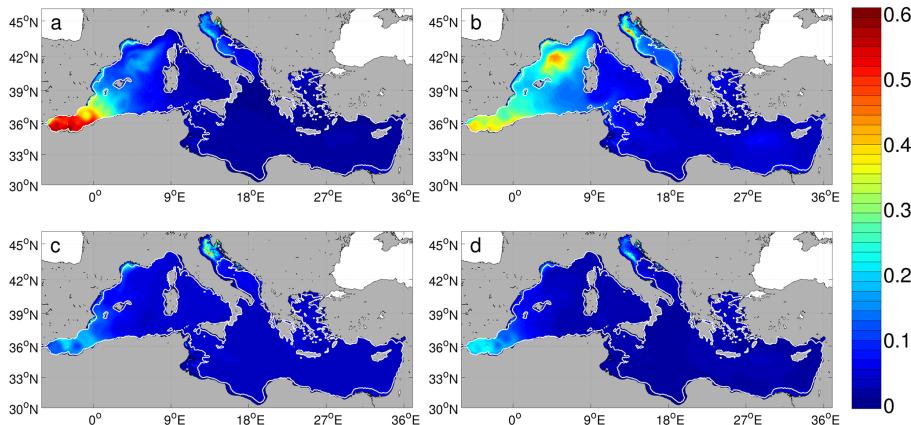
Figure 14. Modeled particulate organic carbon inventory ($mol\,m^{-2}$) integrated over the first 100 m. Maps are averaged over the 2000–2012 period on every season (**a**: winter, **b**: spring, **c**: summer, **d**: autumn). White lines are the 0 and 100 m isolines.

Title Page

Abstract · Introduction

Conclusions · References

Tables · Figures

|◄ · ►|

◄ · ►

Back · Close

Full Screen / Esc

Printer-friendly Version

Interactive Discussion
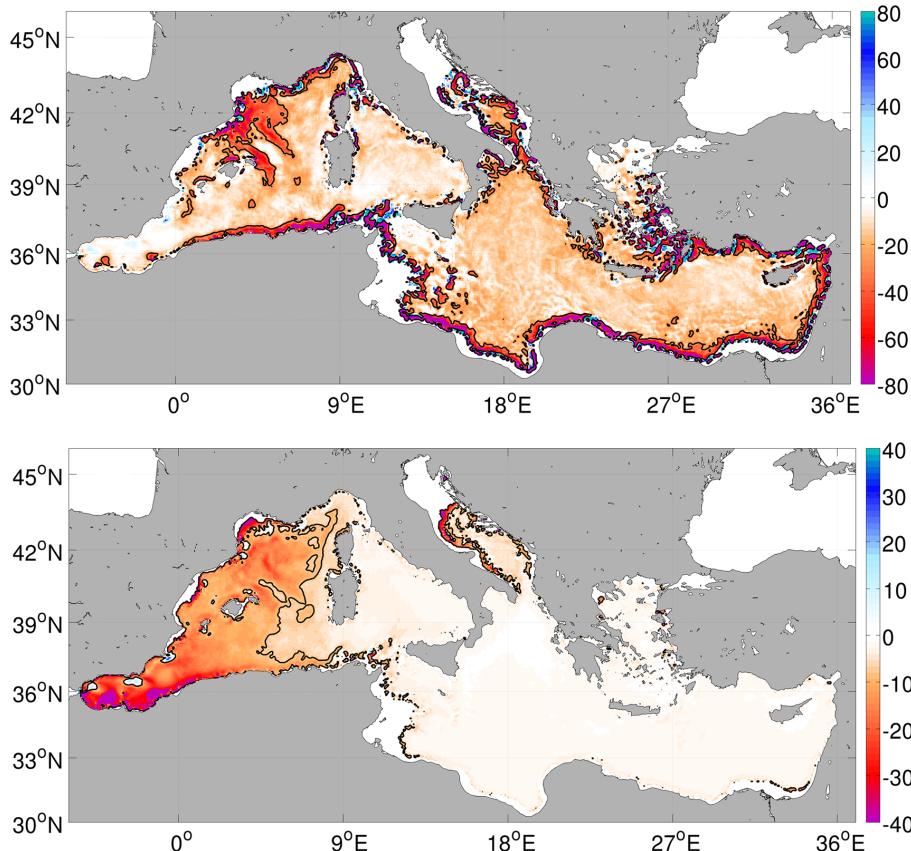
Figure 15. Maps of modeled annual DOC fluxes (top) and POC fluxes (bottom) below the 100 m layer in $g\,C\,m^{-2}\,y^{-1}$. Note the colorscale differences. Negative (red) means a downward flux. Black lines are the contour of the 8th decile of downward fluxes for DOC ($-28.3\,g\,C\,m^{-2}\,y^{-1}$) and for POC ($-7.8\,g\,C\,m^{-2}\,y^{-1}$).

Title Page

Abstract | Introduction

Conclusions | References

Tables | Figures

◀ | ▶

◀ | ▶

Back | Close

Full Screen / Esc

Printer-friendly Version

Interactive Discussion
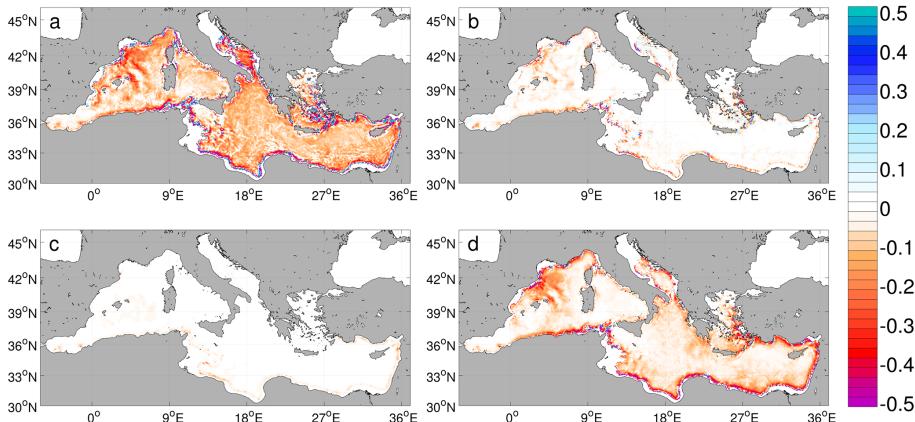
Figure 16. Maps of modeled DOC fluxes across the 100 m layer (F_{DOC}) in g C m^{-2} y^{-1} in winter **(a)**, spring **(b)**, summer **(c)** and autumn **(d)**. Negative (red) means a downward flux.

Title Page

Abstract | Introduction

Conclusions | References

Tables | Figures

◄ | ►

Back | Close

Full Screen / Esc

Printer-friendly Version

Interactive Discussion
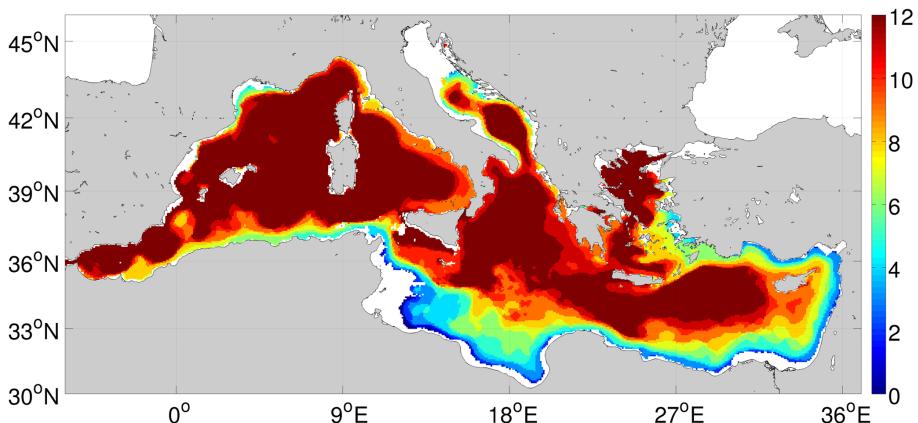
Figure 17. At 100 m depth, number of months over the year during which modeled heterotrophic bacteria C relative quotas is lower than N and P relative cellular quotas.
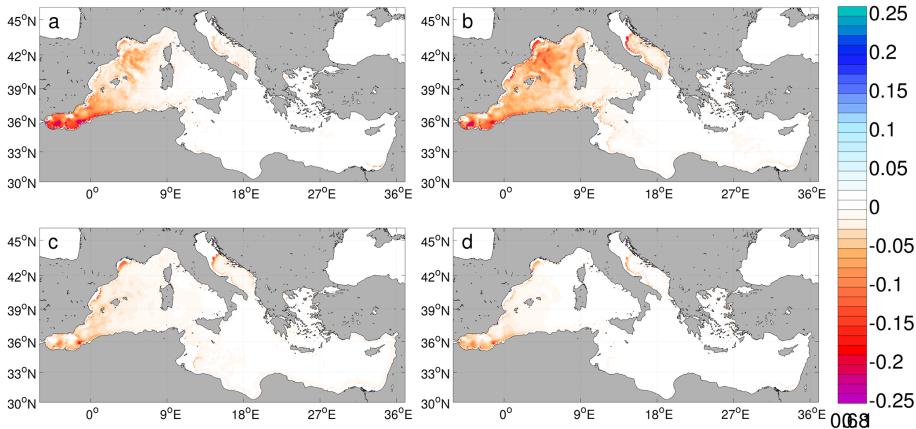
Figure 18. Maps of modeled POC fluxes across the 100 m layer F_{POC} in $\mathrm{g\,C\,m^{-2}\,y^{-1}}$ in winter **(a)**, spring **(b)**, summer **(c)** and autumn **(d)**. Negative (red) means a downward flux.
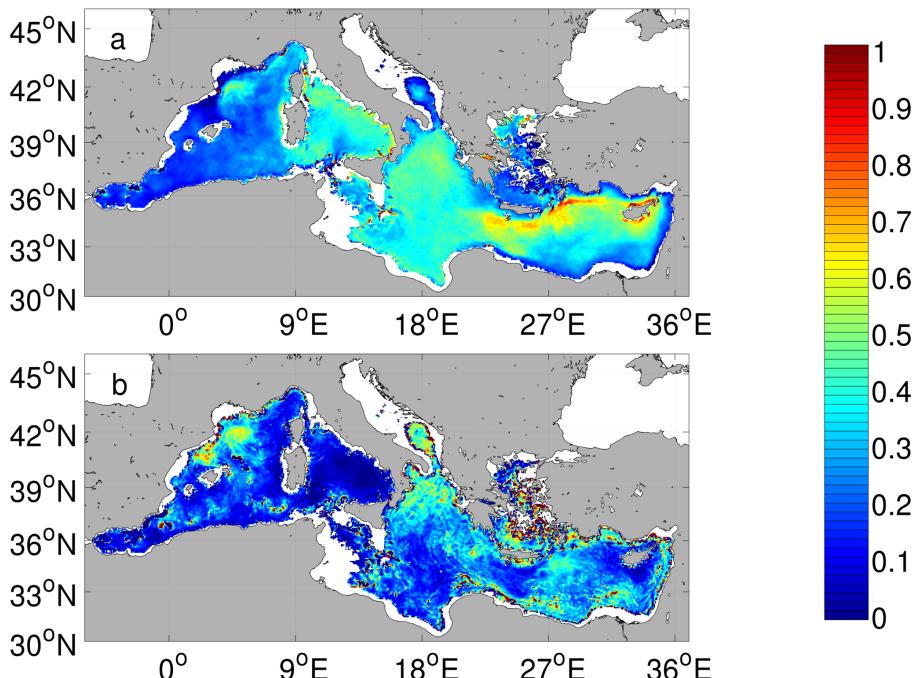
Figure 19. Ratio between export fluxes at 200 m and at 100 m **(a)** for POC, **(b)** for DOC.

Title Page

Abstract | Introduction

Conclusions | References

Tables | Figures

|◄ | ►|

◄ | ►

Back | Close

Full Screen / Esc

Printer-friendly Version

Interactive Discussion